Available online at www.sciencedirect.com
ScienceDirect
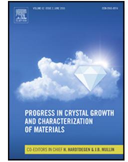

Progress in Crystal Growth and Characterization of Materials 62 (2016) 89–110
www.elsevier.com/locate/pcrysgrow

Review

Fundamentals and engineering of defects

Peter Rudolph *

Crystal Technology Consulting, Helga-Hahnemann-Str. 57, Schönefeld D-12529, Germany

Available online 1 June 2016

Abstract

An overview of the important defect types, their origins and interactions during the bulk crystal growth from the melt and selected epitaxial processes is given. The equilibrium and nonequilibrium thermodynamics, kinetics and interaction principles are considered as driving forces of defect generation, incorporation and assembling. Results of modeling and practical in situ control are presented. Strong emphasis is given to semiconductor crystal growth since it is from this class of materials that most has been first learned, the resulting knowledge then having been applied to other classes of material. The treatment starts with melt-structure considerations and zero-dimensional defect types, i.e. native and extrinsic point defects. Their generation and incorporation mechanisms are discussed. Micro- and macro-segregation phenomena – striations and the effect of constitutional supercooling – are added. Dislocations and their patterning are discussed next. The role of high-temperature dislocation dynamics for collective interactions, like cell structuring and bunching, is specified. Additionally, some features of epitaxial dislocation kinetics and engineering are illustrated. Next the grain boundary formation mechanisms, such as dynamic polygonization and interface instabilities, are discussed. The interplay between facets, inhomogeneous dopant incorporations and twinning is shown. Finally, second phase precipitation and inclusion trapping are discussed. The importance of in situ stoichiometry control is underlined. Generally, selected measures of defect engineering are given at the end of each sub-chapter.
© 2016 Elsevier Ltd. All rights reserved.

Keywords: melt structure; point defect; segregation; constitutional supercooling; dislocation; dislocation dynamics; thermomechanical stress; grain boundary; facet; twin; precipitates; inclusion

1. Introduction

An overview of the important defect types, their origins and interactions during the bulk crystal growth from the melt and epitaxial processes is given. The attention is focused on semiconductor crystals but the knowledge can be applied to other material classes too.

After defect classification the treatment shows selected thermodynamical and melt-structure considerations. Then zero-dimensional defect types, i.e. native and extrinsic point defects, are introduced. Especially, their electrical activity and interchange are discussed. The striation genesis and effect of constitutional supercooling are added.

Dislocations and their patterning are discussed next. The role of high-temperature dislocation dynamics for collective interactions, like cell structuring and bunching, is specified. Additionally, the central issues of heteroepitaxy and their control, like arising stresses, bowing, cracking, misfit dislocations and dislocation bending, are specified.

Next the grain boundary formation mechanisms, such as dynamic polygonization, interface instabilities and multinucleation, are depicted. The interplay between facets, inhomogeneous dopant incorporations and twinning is demonstrated.

* Crystal Technology Consulting, Helga-Hahnemann-Str. 57, Schönefeld D-12529, Germany. Tel.: 0049 3379 444253.
E-mail address: rudolph@ctc-berlin.de.

http://dx.doi.org/10.1016/j.pcrysgrow.2016.04.004
0960-8974/© 2016 Elsevier Ltd. All rights reserved.

Finally, second phase precipitation and inclusion trapping are discussed. The importance of in situ stoichiometry control is underlined.

It is noteworthy that in the past the author presented related lectures at various international schools of crystal growth such as ISSCG-13, ISSCG-15 and IWCGT-3. He also published numerous reviews on crystal defects in journals, conference proceedings and handbooks, see e.g. refs. [1–5]. Thus, in the present chapter only an excerpt of the most important facts is given. For deepening studies the reader may refer to these publications and the literature listed at the end of the paper.

2. Defect classification

Crystal defects, entered in Table 1, are usually classified according to their dimensions.

Zero-dimensional defects are *point defects* comprising intrinsic types like vacancies, interstitials, and, in compounds, antisites as well as unintentionally or intentionally introduced extrinsic atoms as impurities or dopants, respectively.

One-dimensional defects include all kinds of *dislocations*, such as screw and edge dislocations, mixed dislocations, partial dislocations, and dislocation loops. At epitaxial processes one differs between misfit and threading dislocations showing defect lines parallel to the substrate–layer interface and perpendicularly by growing together with the layer surface through the whole epitaxial system, respectively.

Two-dimensional defects are *grain boundaries*, *stacking faults*, *phase boundaries*, *facets*, and *twins*. Low-angle grain boundaries and dislocation cells with tilt angles in the region from arcsec to arcmin, belonging conventionally still to a single crystalline state, are formed by dynamic polygonization and dissipative structuring. In contrast, large-angle grain boundaries with tilt angles of some degrees are formed by polycrystalline growth. Usually, the indication polycrystal is used above tilt angles of 11–15° when the grain boundary energy loses its dependence on the degree of grain tilt. Facets appear along atomically smooth planes. Their very rapid and discontinuous layer-by-layer growth mechanism incorporates impurities in enhanced concentration and may stochastically create twins by faulty planar nucleus stacking.

Three-dimensional defects include second-phase *particles* (precipitates), intrinsic vacancy conglomerates (microvoids), and foreign particles or bubbles (inclusions). *Precipitate*s and *microvoids* are formed by condensation of intrinsic point defects, whereas *inclusions* are melt-solution droplets, gas bubbles, and foreign microparticles incorporated at the growing interface.

Mostly, the kinetics of the defect classes is interlinked. For instance, the conglomeration of vacancies forms spatial microvoids. The climb of dislocations requires the absolute assistance of point defects. Low-angle grain boundaries are formed by dislocation dynamics, etc.

Table 1
Structural crystal defects classified according to their dimensions.

0-dimensional defects *Thermodynamic equilibrium*	Atomic size (“point“) defects – intrinsic (vacancies, interstitials) – extrinsic (dopants)
1-dimensional defects *Thermodynamic non-equilibrium*	Dislocations – edge, screw, 60°, 30°, mixed – mobile, sessile, bunched
2-dimensional defects *Thermodynamic non-equilibrium*	Stacking faults, twins Grain and phase boundaries Facets
3-dimensional defects *Thermodynamic non-equilibrium*	Precipitates, inclusions Microvoids (vacancy agglomerates) Bubbles, dislocation clusters

3. Thermodynamic considerations

Principally, defects exhibit heightened energetic potential. In comparison with ideal crystal structure dislocations, grain boundaries and second phase particles show a marked energetic excess. Thus, there is a gain of energy (enthalpy) when such imperfects can be reduced or even prevented. In contrast, in all crystals and thin films a small content of point defects is always situated in thermodynamic equilibrium producing certain disorder, i.e. increasing entropy, that leads proportionally to the reduction of potential of Gibbs $G = H - TS$, with H – enthalpy, T – absolute temperature and S – entropy. For instance, in a crystal with constituents or vacancies the energetic minimum occurs when a certain content n^* is presented as

$$n^* = N \exp(-E_d / kT) \tag{3.1}$$

with N – total number of sites in a crystal lattice, E_d – point defect formation energy and k – Boltzmann constant [4,6] (Fig. 1). Thus, a crystal absolutely free of point defects could never be realized. This is all the more true when considering the marked portion of non-equilibrium point defects frozen in the course of the crystal cooling from growth temperature down to room temperature (Fig. 1).

The general thermodynamic principle of energy minimization is responsible for collective interaction of stored dislocations in as-grown crystals and thin films. The formation of dislocation junctions and walls reduces the

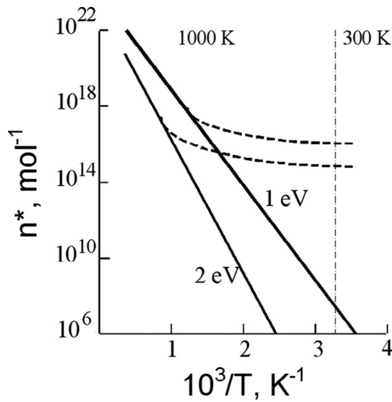

Fig. 1. Two equilibrium curves of minimum defect concentrations $n^* = N \exp(-E_d/kT)$ with defect formation energies $E_d = 1$ and 2 eV vs. reciprocal temperature 10^3/T following Eq. (3.1). The dashed lines show the non-equilibrium ("frozen") curves obtained in reality due to decreasing defect diffusivity with decreasing T.

crystal enthalpy, markedly resulting in gain of energy of each individual dislocation. However, there arises the question is it not true that the resulting dislocation networks should decrease the system entropy by such sorting processes? The answer is "no" due to the acting irreversible thermodynamics. In reality each crystallization proceeds only near thermodynamic equilibrium but never exactly in it. A potential phase difference (supersaturation) is required. In order to meet this preposition a *crystal growth system is an open one* characterized by continuous import and export of energetic flows from a heat source into the growth system and outwards through container walls. After Prigogine [7] such *quasi non-equilibrium thermodynamic situation* produces continuous entropy ($dS > 0$) whereupon maximum entropy ($dS = 0$) is never reached, and thus *conditions of ordering* do exist. As a result the so-called "dissipative structures" can be formed. For example, convection patterns in fluids, cellular ("honeycomb") morphology of propagating solid–liquid interfaces and dislocation cell sub-structures belong to such characteristic phenomena of *irreversible thermodynamics*.

4. The influence of fluid phase

For many years it is well known that there are stabile associates and even structuring phenomena in the fluid mother phases. For instance, in vapor at given materials, temperature and pressure, numerous elements appear as molecules, such as S_2, Te_2, As_2, As_4, etc., and even molecule species like CO, Si_2C, NbO_2, MoO_3, etc. It is one of the main tasks at epitaxy of GaAs and GaN to understand and control the dissociation mechanism of As_n and NH_2/NH_3 molecules within the adsorption layer, respectively. Many modeling and in situ measurements have been carried out to study the association–dissociation kinetics on the growing surfaces of epitaxial layers and possible harmful incorporation mechanisms of the presented species.

Due to the much higher density in fluxes and melts, the trend toward association is here more pronounced than in vapor. For example, the first principle numeric modeling showed that at growth of GaN crystals from Na–Ga flux, the bonding of nitrogen atoms with two Ga atoms leads to undesirable pre-nucleation already within the solution bulk even far from the GaN seed. It has been found that at doping of $<10^{17}$ cm^{-3} carbon atoms in the flux, the formation of stable CN^- ions suppresses the spontaneous nucleation on any area other than the substrate [8].

More difficult is the situation in multi-component melts. As it is well known the higher is the bond ionicity f_i of a given material system the lower is the degree of dissociation α_d within the fluid [9]. For instance, the III–V compounds with low f_i values < 0.4, like GaAs, GaSb, and InSb, show metallic character with very high α_d (>0.9) in the molten state. Thus, dissociated III and V atoms are presented immediately at the crystallization front. Thus, it can be assumed that separated A and B atoms are assembling a well-ordered crystal lattice. Another situation occurs in highly ionized compounds, such as II–VIs (CdTe, ZnTe), showing very low degrees of dissociation (<0.05) and still semiconducting behavior of the melt. In such case molecular building blocks enter the crystallization front, like CdTe and Cd_2Te_3 at tellurium mole fraction $x_{Te} = 0.5$ and 0.8, respectively [10]. That may markedly affect the correct crystal assembling and second phase precipitation. In fact, in II–VI crystals a much worse defect density (twinning, dislocations, precipitates), then in III–Vs, is usually obtained. Especially at the growth of biological crystals, such as proteins, the huge macromolecular building units within the solution showing diameters up to 20 nm are nearly non-penetrable. Once such macromolecules approach the growing crystal surface they have to rotate until they find the proper orientation into the crystal geometry. Otherwise, when a growth unit is immobilized in the crystal structure before it finds the correct fit, an orientational defect is created, deteriorating the quality of the crystal lattice [11]. In order to enhance the adaptability of such macromolecules, a proper control of the solution parameters like concentration, supersaturation, mass transport and external magnetic fields is required [12].

The situation is being further deteriorated by possible melt structuring in the form of chains, rings and, like

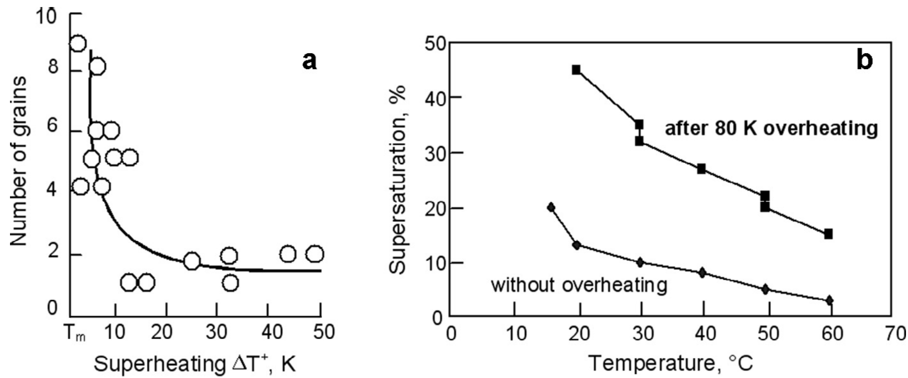

Fig. 2. (a) The number of misoriented grains over the whole ingot of VB CdTe crystals vs. melt superheating over the melting point T_m before the crystallization was started (adapted from Ref. [2]). (b) Rapid growth with 16 mm/d of high-quality KDP crystals in highly supersaturated aqueous solution obtained at superheating of 80 K over 24 h before the growth was started (adapted from Ref. [15]).

in II–VI, by the presence of residual tetrahedrons [13]. Such configurations cannot only induce marked lattice defects but also control the crystal orientation. For instance, there is a distinct self-orientation of CdTe crystals (mostly along <110 > and <221> growth directions) independently whether a seed is used or not. That means, at a <100> -oriented seed this direction is not continued by the growing crystal and the orientation is immediately changed toward <111> and <221>. The author assumes that for this phenomenon the melt structure is responsible. Further he found out, that the overheating of the melt and holding time are decisive factors to reduce structural formations and improve the crystal quality [14] (Fig. 2a). Today, the growth of CdTe and (Cd, Zn)Te crystals from well-overheated melts becomes a worldwide standard (e.g. [15]). For comparison, also at growth from aqueous solution, high-quality KDP crystals have been only obtained when subcritical clustering was destroyed by large superheating settled over 24 hours before the crystallization was started [16] (Fig. 2b).

Therefore, we can conclude that much more attention must be devoted to the correlation between melt “structure” and possible crystal defect formation.

5. Selected point defect phenomena

5.1. Intrinsic point defect balance

Generally, at all temperatures above absolute zero, equilibrium concentrations of vacancies V, self interstitials I and, in the case of AB compound crystals, anti-site defects A_B and B_A will exist. This is because the presence of point defects contributes to increase the configurational entropy leading to a decrease in free energy of the crystal (see section 3). Theoretically, only a certain equilibrium point defect content around 10^6–10^9 cm^{-3} is estimated for room temperature. However, in reality a much higher non-equilibrium point defect concentration is presented at 300 K even in high-purity crystals (10^{14}–10^{16} atoms per cm^3). This is due to the limitation of finite defect diffusion rate leading to the freezing-in of a considerable part of the high-temperature defect concentration during the crystal cool down (Fig. 1). On the other hand, at sufficient high temperature and time buffer annihilation of vacancies and interstitials can occur. Thus, the real point defect concentration is dependent on the crystal growth conditions, such as cooling rate modifying with applied temperature gradient and growth velocity, as well as with deviation from stoichiometry in compound materials. Hence, the crystal grower must obtain an understanding of native point defect situation very carefully in order to carry out accurate defect engineering.

During crystal pulling or unidirectional solidification from the melt, the native point defects undergo various types of transport kinetics, i.e. capture at the propagating interface (often designated as “convection”), Fickian diffusion within the crystal, and temperature-gradient-driven thermal diffusion (Soret effect). Until now the case for dislocation-free silicon monocrystals grown from melt by Czochralski or floating zone is the situation studied best [17]. At the growing melt–solid interface there are point defects of about 10^{14} cm^{-3} whereupon the vacancy concentration $[V]$ is always slightly higher than the interstitial content $[I]$. However, the interstitial diffusivity $D_I = 5 \times 10^{-4}$ cm^2 s^{-1} exceeds that of vacancies $D_V = 3 \times 10^{-4}$ cm^2 s^{-1}. Therefore, at low pulling rates, interstitials are in excess forming a network of dislocation loops. In contrast, at high growth rates the vacancy flux is dominating over the interstitial flow, leading in

consequence to the condensation of vacancy agglomerates (microvoids). In between both defect kinds are minimized due to recombination. The controlling factor proves to be the ratio between growth velocity v and axial temperature gradient G to be in silicon $v/G = 1.38 \times 10^{-3}$ cm^2 min^{-1} K^{-1} [18]. When the experimental v/G values are close to this critical ratio, like in standard Czochralski processes, the crystal contains often both interstitial and vacancy dominated regions at the periphery and center, respectively. This is caused by the radial variation of the temperature gradient increasing from the center toward the rim. In mass production the process time proves to be a decisive factor. In place of uneconomical low pulling rates to respect the critical v/G condition (±10%), a maximum pulling rate with fast cooling followed by a wafer annealing process to reduce the grown-in defect sizes or covering the microvoids by "flash epitaxy" of an Si thin film seem to be economical alternatives. To find out the optimum point defect engineering for growth and after treatment of the aimed 18 inch (450 mm) generation proves to be the next challenge because with increasing crystal diameter the value of G is reduced [19], and thus the interstitial content enhanced.

In compound crystals the intrinsic point defect balance is additionally influenced by the deviation from stoichiometry. Depending on the temperature and atomic interaction energies, the solubility of point defects of the given excess component deviates more or less from stoichiometric composition forming the *region of existence* $A_{\delta B}B_{\delta A}$ in the phase diagram, with $\delta B, \delta A$ the mutual maximum solubilities, i.e. the solidus courses. A non-stoichiometric composition enhances not only the formation of excess vacancies or interstitials but also antisites. Their ratio to each other determines the compensation level, type of conductivity, carrier concentration, absorption behavior, diffusivity, efficiency of dopant incorporation, etc. Intrinsic point defects decorate dislocations being typically for compound crystals and promote their multiplication and mobility. Finally, the characteristic retrograde course of the boundaries of the compound existence region results in the precipitation of excess component during the cooling down process (see section 8). Altogether, as was pointed out in section 2, point defects promote the dynamics of higher ordered defect types.

At high temperatures near the melting point the point defects are isolated and usually electrically charged. This promotes the interaction between opposite charged defects and presented foreign ions (dopants, impurities) to form complexes with reduced degree of ionization or neutrality. Additionally, the influence of the electron or hole concentration generated by charged foreign atoms X^z on the charge state of the native point defects I^z, V^z, $A_B{}^z$ and $B_A{}^z$ is named the *Fermi level effect* [20], whereby the degree of ionization z depends on the position of the Fermi level E_F within the band gap ΔE_g (Fig. 3). For instance, the charge state of the Ga vacancy in GaAs crystal changes from neutral $V_{Ga}{}^o$ in p-type material over double negatively charged $V_{Ga}{}^{2-}$ in the midgap to a triple negatively charged $V_{Ga}{}^{3-}$ in n-type material affecting the compensation level and complex formation probability (see Fig. 3).

Currently, the understanding and control of surface kinetics at epitaxial processes of GaN layers are among the key targets of crystal growth. According the related ab initio simulations of Kempisty et al. [21] on HVPE growing (0001) GaN planes, there is an interplay between E_F position and adsorption energy of the Ga atoms. Increasing the acceptor doping concentration, and thus the

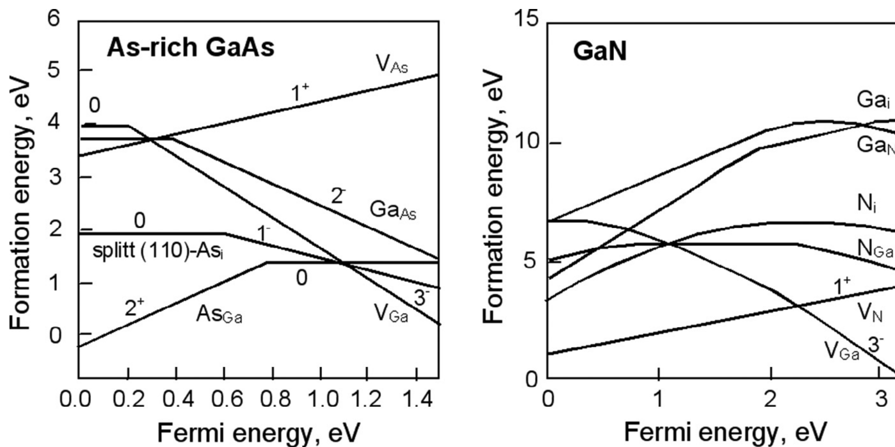

Fig. 3. Dependence of native point defect formation energies and ionization levels on the Fermi energy in As-rich GaAs and GaN (adapted from Ref. [5]).

shift of E_F toward valence band, the Ga adsorption at the correct site of the wurtzite lattice structure is enhanced.

5.2. *Intrinsic point defect engineering*

The in situ control of native point defects in compound crystals is coupled with the feasibility of accurate composition control during the growth process, and therefore with the exact knowledge of the phase diagrams. If highly purified material is used near-stoichiometric high-resistivity compound crystals can be obtained caused by intrinsic defect annihilation. Well known for a long time is the application of a temperature-fixed vapor source of the volatile component during horizontal Bridgman (HB) method without covering of the melt [22]. In this technique, there is a direct contact of the vapor phase with the crystallizing melt–solid phase region that guarantees near-phase equilibrium condition during the whole growth run. Also the vertical Bridgman (VB) and vertical gradient freeze (VGF) techniques were introduced by using an extra source for the vapor phase control [23]. Vapor pressure-controlled HB, VB and VGF have been successfully used to grow near stoichiometric compound semiconductors, like CdTe [24] and GaAs crystals, the last even without boric oxide encapsulation of the melt surface [25]. Even at Czochralski growth of GaAs the stoichiometry control has been tested by using the vapor pressure-controlled Czochralski (VCz) technique [26]. It was demonstrated that near-stoichiometric growth condition with a Ga-rich melt reduces both the As_{Ga} antisite and V_{Ga} concentrations [27]. Also as a relatively rare case an in situ vapor phase control at Czochralski growth of oxide crystals (e.g. $PbWO_4$) has been described [28]. The optical transmission was markedly improved.

However, both the own segregation behavior of the intrinsic point defects when they are captured at the propagating interface (section 5.3), and their enhanced complex formation probability with axially increasing extrinsic defect concentration, make the overall control of stoichiometry during the whole growth run very complex. Nevertheless, the development of a well-controlled temperature program of the extra source $T_Q(t)$ being well fitted with the actual growth rate v would guarantee a constant near-stoichiometric growth situation. For instance, already in ref. [24] the author presented the thermodynamically estimated $T_Q(v)$ curves for VB and VGF growth of CdTe. They could be used to devise a related $T_Q(t)$ program. At the present, however, the stoichiometry is still corrected in cut wafers by post-growth annealing, especially to minimize the precipitate density of the agglomerated excess component [29,30].

5.3. *Extrinsic point defects incorporation*

As was introduced in section 1 the extrinsic point defect term describes unintentionally and intentionally presented foreign atoms as residual *impurities* and *dopants*, respectively. They occupy interstitial or substitutional (lattice) positions. In growing crystals with dopant concentrations below the solubility limits, the matrix is regarded as contributing in a phase diagram one component and the solute another. Thus, the system can be considered as a binary one. The equilibrium between the chemical potentials μ of the species i involved in the liquid (i.e. solvent) l and solid s phases $\mu_{il}(x,T) = \mu_{is}(x,T)$ yields

$$\mu_{is}^o + kT\ln x_{is}\gamma_{is} = \mu_{il}^o + kT\ln x_{il}\gamma_{il} \tag{5.1}$$

with x the mole fraction, T the absolute temperature, μ^o the standard potential, and γ the interaction activity between i and atoms or molecules of the matrix. Setting $\mu^o_{il} - \mu^o_{is} = \Delta\mu^o_i = \Delta h^o_i - \Delta s^o_i T$ and $s_i^o = h_i^o/T_{mi}$, with h_i^o, s_B^o the intensified standard enthalpy and entropy, respectively, T_{mi} melting point of the dopant, and $\Delta h^o_{Mis,l} = kT \ln\gamma_{is,l}$ the mixing enthalpy, the transformed equation (5.1) becomes [31]

$$\frac{x_{is}}{x_{il}} = k_o = \exp\left[-\frac{\Delta h_i^o}{k}\left(\frac{1}{T}-\frac{1}{T_{mi}}\right)+\frac{\Delta h_{Mil}-\Delta h_{Mis}}{kT}\right] \tag{5.2}$$

with $k_o = x_{is}/x_{il}$ the (thermodynamic) *equilibrium distribution* (or *segregation*) *coefficient*, which can be assumed as a constant for residual impurity or low dopant concentrations if the solidus and liquidus curves allow their linearization.

The homogeneous redistribution of dopants (and also impurities) along the growing crystal proves to be a great challenge for the crystal grower. The deviation of the equilibrium distribution coefficient k_o in Eq.(5.2) from unity causes segregation phenomena during melt and solution growth, which can be treated in terms of an effective segregation coefficient $k_{eff} = x_{is}/x_{il}^{(\infty)}$ with $x_{il}^{(\infty)}$ the mole fraction of the dopant or impurity in the fluid far away from the crystallizing interface. During the solidification process the solute is rejected ($k_o < 1$) or preferentially absorbed ($k_o > 1$) by the propagating solid–liquid interface, forming an enriched or depleted diffusion boundary layer of the component i in front of it. The width δ_D of this boundary layer is determined by the growth velocity v and by the diffusive and convective species transport in the melt, which is very often difficult to predict (note, a detailed discussion of the quantification of the δ_D value in dependence on the melt convection regimes is given in the recently published review of Ostrogorsky

and Glicksman [32]). A very popular model that is commonly used in melt growth was introduced by Burton, Prim and Slichter (BPS) [33] for the steady state of segregation

$$k_{eff} = \frac{k_o}{k_o + (1-k_o)\exp(-v\delta_D / D)} \tag{5.3}$$

with D the diffusion coefficient in the melt.

Thus, in dependency on the value of δ_D the effective separation of extrinsic point defects at a growing interface k_{eff} becomes an indicator for the degree of melt mixing. In case of complete melt mixing the axial distribution of a given impurity or dopant along a directionally solidified crystal ingot is then approximated by the formula of Scheil [34]

$$x_{is} = x_{io} k_{eff} (1-g)^{k_{eff}-1} \tag{5.4}$$

with x_{io} the starting mole fraction of the impurity/dopant, $g = z/L_o$ the solidified fraction (L_o – length of the charge, z – distance from the initial growth face). As can be seen, the highest axial chemical homogeneity, also named *macroscopic distribution uniformity*, is obtained when k_{eff} approaches unity, requiring, however, a high as possible growth velocity or convection-less diffusion-driven mass transport regime (note, in section 5.4 will be shown that v cannot increased infinitely). Further, at pure diffusion-limited case Scheil's equation should be replaced by Tiller's distribution function [35] and for zone melting by Pfann's relation [36]. Finally, Eq. (5.4) is valid only for conservative crystal growth systems where no any masses are exchanged. In reality, of course, there is always a certain evaporation and adsorption at the melt surface varying x_{io}. For such non-conservative HB case Madelung [37] modified Scheil's Eq. (5.4) as following

$$x_{is} = x_{io} k_{eff} (\alpha + 1 - g / \alpha + 1)^{k_{eff}-1} \tag{5.5}$$

with $\alpha = V/SL_o k_{\mathrm{vl}}$ (V – volume of gas phase, S – cross section of growing interface, $k_{\mathrm{vl}} = x_{iv}/x_{il}$ – separation coefficient between vapor and liquid phase). On the other hand, in order to enhance the axial homogeneity, a non-conservative regime can be applied to dope intentionally in situ from the working atmosphere. At liquid encapsulated Czochralski (LEC) growth of GaAs a controlled carbon doping has been achieved in order to obtain homogeneous high-resistivity material by compensating the intrinsic EL2 (As_{Ga}) defects. The C atoms are incorporated from the melt via decomposition of delivered gaseous CO molecules at the interface between boric oxide encapsulant and Ga–As melt [38,39]. A non-conservative coupling factor α' consisting of the CO diffusion coefficient within boric oxide, the height of encapsulant and the ratio between crucible and crystal radius was added to Scheil's formula [39]. Fig. 4 compares the theoretical and experimental axial C distribution along the LEC and VCz GaAs crystals [26].

When the temperature of the melt is fluctuating by characteristic convective oscillations according Eq. (5.3) also k_{eff} is oscillatory too. As a result transversal impurity or dopant *microinhomogeneities* ("striations") within the crystal are generated. After Hurle and Jakeman [40] the amplitudes of the compositional fluctuations within the solid $\Delta x_{\mathrm{is}}/x_{\mathrm{is}}$ correlate with the amplitude of velocity oscillation $\Delta v/v$ and perturbation frequency f as

$$\frac{\Delta x_{is}}{x_{is}} = \frac{\Delta v}{v}(1-k_o)\frac{v\delta_D / D}{(2f\delta_D^2 / D)^{1/2}} \tag{5.6}$$

(δ_{D} – diffusion boundary layer, D – diffusion coefficient in the melt). From this relation follows that at frequencies higher than about 10 Hz the relative concentration fluctuations fall to less than 10%. Therefore, low-frequency fluctuations affect much more the crystal homogeneity than high-frequency ones. In other words, a melt–solid *interface acts as low-pass filter*. Unfortunately, the frequencies of buoyancy convections are typically in the range of 0.1–0.5 s^{-1}. To damp them the flow must be controlled either by well-harmonizing crucible rotation or total convection depression by applying magnetic fields [41].

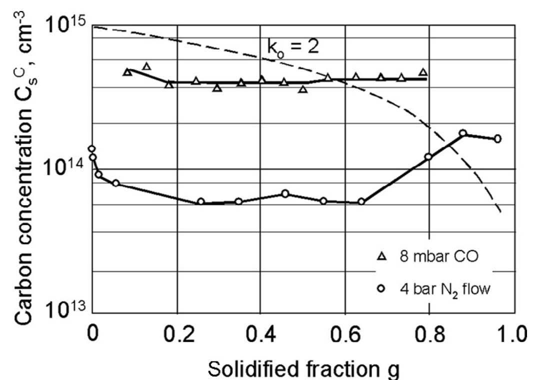

Fig. 4. Axial carbon distribution in LEC (Δ) and VCz (o) GaAs crystals grown under non-conservative conditions by controlled CO gas concentration (8 mbar) and rinsing nitrogen working gas (~4 bar), respectively. The broken curve shows the theoretical Scheil distribution with $k_o = 2$ (the equilibrium segregation coefficient of carbon) in case of conservative growth regime with complete melt mixing ($k_o = k_{eff}$) and starting concentration $x_{Co} = 5 \times 10^{14}$ cm^{-3} (adapted from ref. [4]).

5.4. Constitutional supercooling

Constitutional supercooling is one of the remarkable point-defect-induced origins generating polycrystalline growth, and thus a complete production loss. Under certain conditions, when the diffusion boundary layer δ_D of a solute is well developed, e.g. if there is no enough melt mixing, the interface can become morphologically unstable. Both an enriched ($k_o < 1$) or depleted ($k_o > 1$) solute layer δ_D, showing a typically exponential concentration dependence (increasing or decreasing, respectively), give rise to constitutional instability, especially in the case if the corresponding liquidus temperatures of the concentration course exceed the actual temperature course (Fig. 5a). Then random formation of a protrusion on the interface advances that portion of the interface into the region of increased supercooling. Here, it can grow more rapidly causing a lateral segregation of solute that suppresses growth in the neighboring region. As a result, a close packed array of such protrusions forms with a length scale of the lateral diffusion distance *D/v*. Such cellular interface morphology, which can be related to a *dissipative structure*, produces harmful columnar grain boundary structures with redistributed concentration and dislocation densities leading, finally, to polycrystallinity.

Note, constitutional supercooling can be also caused by a component excess at growth of compound crystals under non-stoichiometric conditions (see Fig. 5b). The rejection of the excess atoms lowers the liquidus temperature before the growing interface in exactly the same way as a solute and the danger of polycrystalline growth is comparatively high [4].

After Tiller et al. [42] deduced theoretically the condition for prevention of constitutional supercooling by taking under consideration of a critical ratio between temperature gradient G and growth velocity v, Mullins and Sekerka [43] completed this correlation by a linear stability analysis taking into account the difference of thermal conductivity in the solid and molten phases. According to this the onset of morphological instability is prevented when

$$\frac{G}{v} > \left(\frac{m x_{iL}(1-k_o)}{k_o D} - \frac{\Delta H \rho}{\lambda_s + \lambda_l}\right)\left(\frac{2\lambda_l}{\lambda_s + \lambda_l}\right) \qquad (5.7)$$

with the left term in the first bracket as Tiller relation (m – slope of the liquidus in the T-x – phase projection, x_{iL} – mole fraction of given impurity/dopant in the melt, k_o – distribution coefficient, D – diffusion coefficient in the melt, ΔH – latent heat, ρ – density of solid, $\lambda_{s,l}$ – the thermal conductivity of solid and liquid, respectively).

Following this equation, constitutional supercooling can be prevented by a largest possible *G/v* ratio. However, growth under low thermal stress does often limit G and low v proves to be uneconomical. For that reason, special actions against solvent enrichments at the interface must

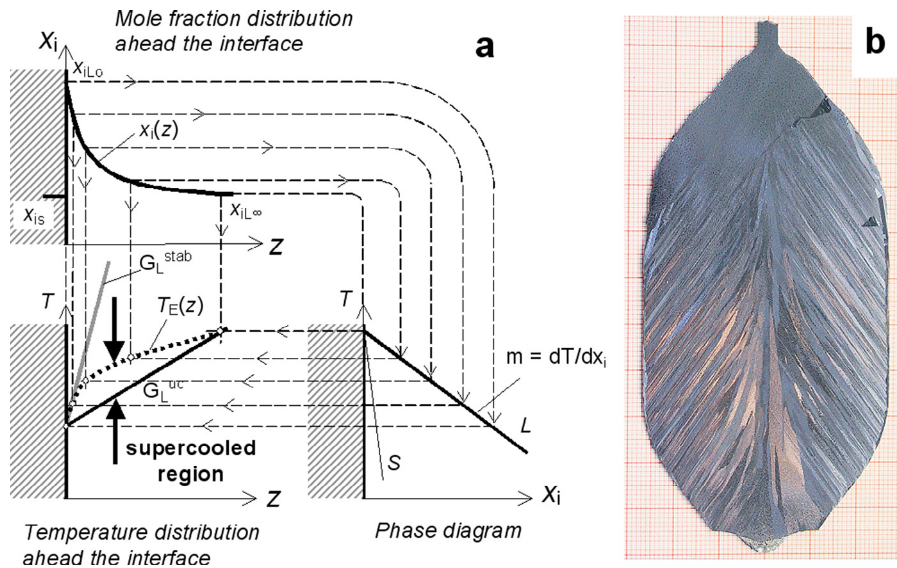

Fig. 5. (a) Graphic construction of the constitutional supercooling (x_{is}, x_{iLo}, $x_{iL\infty}$ – mole fraction of the given impurity/component excess/dopant in the solid, at the growing interface and in the melt, respectively, T – temperature, z – axial coordinate, S – solidus, L – liquidus, T_E(z) – equilibrium temperature distribution ahead the interface, G_L^{uc}, G_L^{stab} – temperature gradient of the furnace in case of undercooling (uc) and at stable condition without undercooling (stab)); (b) Undoped LEC InP crystal with features of morphological instability (cellular interface) grown from In-rich melt with too high pulling rate (courtesy of M. Neubert).

be taken such as artificial melt mixing by accelerated crucible rotation technique, ultrasonic vibration stirring or time-dependent (i.e. rotating, alternating, traveling) magnetic fields as reviewed in ref. [41]. In case of compound growth the excess of one component in the melt can be prevented by *in-situ stoichiometry control* via partial pressure regulation over the melt (see section 5.2).

6. Dislocations

6.1. Definitions and energetic background

A crystalline material under mechanical or thermomechanical stress first withstands by its *elasticity*. However, such energetically elevated state is a metastable one inducing *deformation and even slip*. When the stress value exceeds a critical one the elasticity is reduced by *plastic deformation* that occurs when the applied shear stress is large enough to overcome the potential energy barriers. At that point, atoms will move from one equilibrium position to the next one. The process is named "slide" [44].

In real crystals, the theoretical value of critical shear stress of plastic deformation is many orders of magnitude greater than the observed values. The difference is attributed to the presence of *dislocations*. They are classified in edge (with Burgers vector normal to the dislocation line), screw (with Burgers vector parallel to the dislocation line), 30°, 60° and mixed dislocations. The Burgers vector may decompose into two *Shockley partials* with stacking fault between partials of the distance $d_{St} = G\,b^2/\gamma_{SF} \sim 1/\gamma_{SF}$ (G – shear modulus, b – Burgers vector, γ_{SF} – stacking fault energy).

Dislocation lines can end at the crystal surface and at grain boundaries, but never inside a crystal. "Endless" dislocation rings are possible. For generation of a dislocation in a homogeneous crystalline body usually an extremely high stress of ~ 10^{-2}–10^{-1} G with G = 10–50 GPa is required. In contrast, much lower stress is needed to move and multiply already presented dislocations. For instance, near the melting point T_m the critical resolved shear stress (CRSS) τ_C to move dislocations is in Si 9 MPa, in GaAs 0.5 MPa, in CdTe 0.2 MPa and in Cu 0.02 MPa. Therefore, at bulk growth the probability of generation of new dislocations is marginal due to the relative low thermal stress, and thus the dislocation density is mainly determined by multiplication of already existing dislocations, e.g. penetrating from the seed. Of course, when second phases inclusions are presented dislocations can be generated at their periphery due to the lattice misfit. Further, dislocation loops are generated when vacancies or interstitials are condensed in the form of discs. Partial dislocations can be obtained at facet boundaries on bulk crystal surfaces [45]. In comparison, at heteroepitaxial processes the much higher misfit stresses can reach values in the region from some hundred MPa up to GPa leading to system bowing and generation of dislocations.

Growth dislocations are connected with the melt–fluid growth front and proceed with it during growth. Sources are the overgrowth of inclusions (section 8) and interface instabilities, like cellular morphology (section 5.4). In comparison, *post-growth dislocations* are generated behind the growth front, either during the growth run or during cooling down process. Sources are melt or solvent inclusions, point defect condensates and wetting at container walls.

Dislocations are sources of internal stress within the crystal. The *elastic energy* of single screw (κ = 1) and edge (κ = 1 – ν) dislocation is

$$E_s = \left(Gb^2 / 4\pi\kappa\right)\ln\left(R / r_o\right) \quad (6.1)$$

with ν the Poisson ratio (the another values are specified within the text above). From this relation follows that E_s drops exponentially with distance from dislocation center (line) yielding at $r = 5b$ still few MPa. Exactly in the center, however, not more describable by linear elastic theory, molecular dynamic simulations revealed maximum local stress up to a few GPa [46] (Fig. 6a).

For nondestructive visualization of individual dislocations extensively the micro photoluminescence (μ-PL) mapping is used. Very high spectral resolution of PL allows the detection of the strain as an energy shift of the donor bound exciton (D°X) around the dislocations. The dipole shape of the strain field is expected for a single edge dislocation where the inserted lattice plane introduces compressive strain on one side of the dislocation and tensile strain on the opposite side [53] (Fig. 6b).

At the present, particular attention is directed on the study of dislocation dynamics in epitaxially grown GaN layers. For example, Forghani et al. [47] demonstrated that μ-PL area scans around edge dislocations in undoped GaN samples show almost a symmetric strain dipole with opposite but identical tensile and compressive peaks. In contrast, in Si-doped GaN crystals asymmetric strain dipoles with reduced compressive pole are formed. As a result a favorable bending down of the dislocation in the course of epitaxy is obtained. In fact, doping can help to transform growth dislocations into basal ones. This is a prime example of the energetic interaction between defects of 0 and 1st order, as underlined in section 2.

The elastic energy of a single dislocation (Eq. 6.1) depends very sensitively on the density of stored

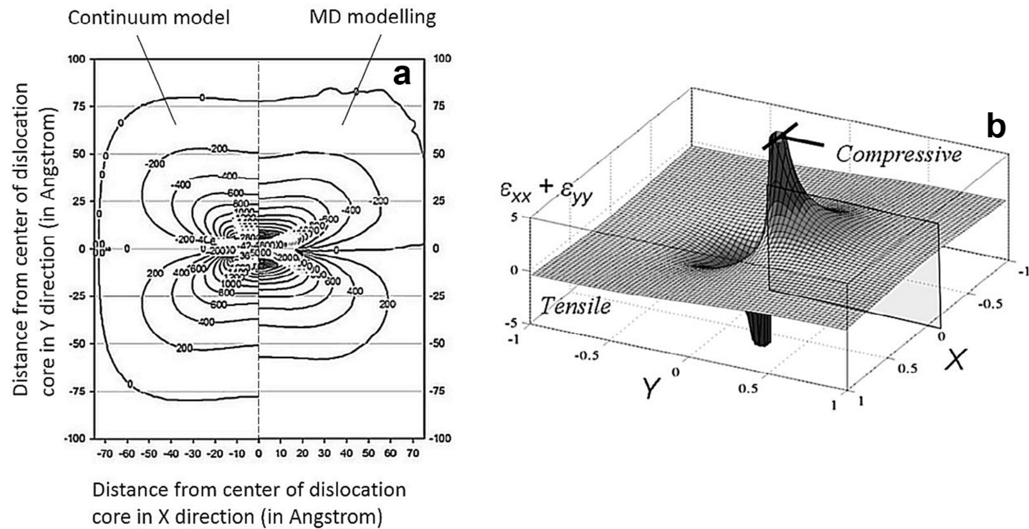

Fig. 6. Stress field around dislocations: (a) σ_{11} component of stress tensor around an edge dislocation in aluminum with results. Left sides of the plot represent the results of the continuum model and the right sides are MD simulation results. The contour plots represent the stress values in MPa (adapted from ref. [46]); (b) μ-PD determined strain dipole $P = \varepsilon_{xx} + \varepsilon_{yy}$ around an edge type dislocation in an undoped GaN layer (adapted from ref. [47]).

dislocation, i.e. on the distance to the dislocation neighbors. Within a dislocation ensemble the self-energy is reduced by the interaction energy named screening effect [54]. Even annihilation takes place when the approaching dislocations along a given plane are of opposite Burgers vectors.

Dislocations move by *glide* and *climb*. Whereas glide is a 2D propagation mode taking place along a given glide plane (e.g. {111} in diamond and zincblende structure), climb is a 3D process based on diffusion-driven docking or release of lattice atoms or vacancies perpendicularly to the dislocation line producing jogs of it. Thus, whereas glide is only driven by the acting elastic stress, climb needs point defects. Due to the retarding diffusivity with decreasing temperature, climb is subjected to high temperatures (i.e. behind the growing interface). In comparison, glide occurs still down to relative low temperatures. For instance, still at about 500 °C glide bands along <110 > directions are generated in GaAs {111} wafers installed for an epitaxial process on a supporting disc showing temperature difference between rim and center.

Of special interest is the energetic situation of growth dislocations immediately at the propagating interface, because near a surface they experience forces not encountered in the bulk [48,55] (Fig. 7a). The dislocation is attracted toward a free surface where the material is more compliant and the dislocation energy is lower. Contrary, at rigid surface the dislocation is repelled. To treat this mathematically, the imaginary stress field of the given dislocation type is added. Such an *image dislocation* is a virtual dislocation situated outside the material, which generates a stress field compensating at the free surface the stress field of the actual inner dislocation. The image force has no effect, for symmetry reasons, on the dislocations when they are perpendicular to a basal surface. On the other hand, they move their lines in the basal plane when they become close enough to an inclined facet. This is of high practical importance for epitaxial processes due to the controllability of the dislocation growth direction. Adjusting an interim 3D growth mode of pyramidal interface morphology the originally perpendicular directed dislocations are bended sideways toward pyramidal facets. As a result the dislocation density is decreased along the crystal thickness [49] (Fig. 7b and c).

6.2. Thermomechanical stress and dislocation density

Independent of the growth method used, the density and distribution of dislocations in as-grown crystals are due to a thermoplastic relaxation of thermally and, to a much lower extent, constitutionally induced stress during growth. But the extent of relaxation depends on the growth method used: the longer the resting time at high temperatures (e.g. at low-temperature-gradient methods, like VGF) the lower the residual strain level. Therefore, the content of dislocations is determined by the (time and space dependent) stress level during growth and the thermophysical and mechanical properties of the solid. The level of thermal stress (and its local and temporal

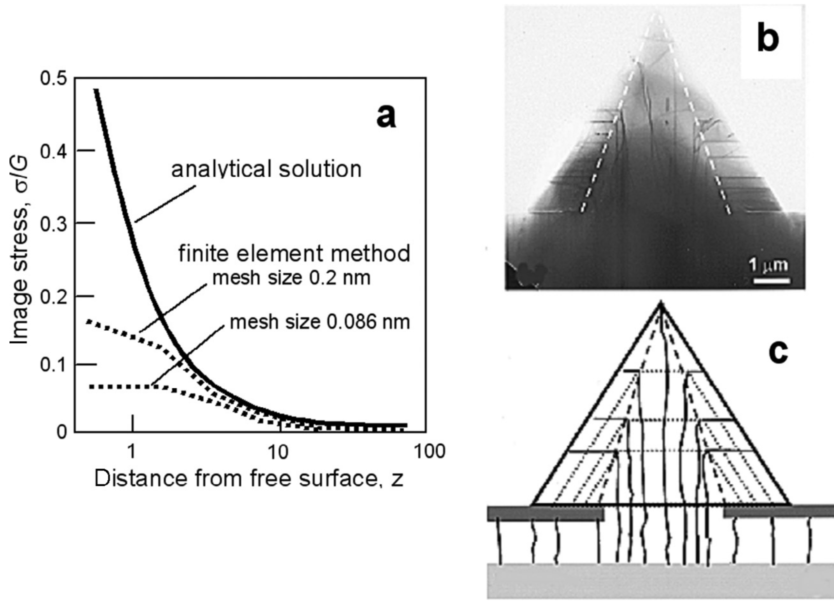

Fig. 7. (a) Calculation of the normed image stresses σ/*G* (*G* – shear modulus) along the dislocation line z (in Angstrom) near the free surface in a semi-infinite fcc medium (adapted from ref [48]); (b) transmission electron micrograph of the dislocation courses in a GaN pyramid grown through a mask window on a sapphire substrate by MOVPE epitaxial lateral overgrowth (ELO), viewed along [10-10] direction; (c) sketch of image in (a). Dotted lines show the {11–22} and (0001) faces in successive ELO stages. The dislocations (full lines), proceeding through the mask window, are bent by 90° into the horizontal (0001) basal plane when penetrating the boundary to the neighbored {11–22} sectors (adapted from ref [49]).

fluctuations) is unambiguously related to the temperature field (including its fluctuations) in the crystal during growth and cooling-down procedure. Hence, the knowledge and control of the temperature field at all process stages are of essential significance. Due to the difficulties of experimental determination the numerical simulation is of highest importance for heat flow analysis and "tailoring" [56].

Knowing the temperature field within the growing crystal consisting of differences ΔT(x,y,z) (here in Cartesian coordinates) the thermal deformation for each coordinate can be deduced by the relation

$$\varepsilon_T(x,y,z) = \alpha_T(T)\Delta T(x,y,z) \quad (6.2)$$

with $\alpha_T(T)$ the linear thermal expansion coefficient as function on absolute temperature T (note $\Delta T = T - T_0$ with T_0 a stress-free constant reference temperature, e.g. melting point T_m). And now it is immensely important to consider that the linear dependence of Eq. (6.2) does not yet induce any thermal stress σ that only begins to act when nonlinear temperature fields are presented as it is typical for each crystal growth system. Thus, the thermal deformation must be complemented by the term of elastic deformation $\varepsilon_\sigma = \sigma$(x,y,z)/$E$ (E – Young modulus), so that the resulting deformation field becomes

$$\varepsilon_\Sigma = \varepsilon_T + \varepsilon_\sigma = \alpha_T(T)\Delta T(x,y,z) + \sigma(x,y,z)/E \quad (6.3)$$

(of course, for more mathematical–physical precision the values must be translated into tensorial versions as they are treated in textbooks of classical theory of elasticity).

Due to the conditions of compatibility of the total deformation $\nabla \times \varepsilon_\Sigma \times \nabla = 0$ (see textbooks of theoretical physics), the generation of thermal stresses is related to the second derivatives of the spatial temperature distributions $\partial^2 T/\partial n^2$, i.e. to "curvatures" of the temperature field and not to the gradient $\partial T/\partial n$ (with n the normal in Cartesian x,y,z or cylindrical r,θ,z coordinates). As it was demonstrated by Indenbom [57] a linear temperature distribution with a constant temperature gradient produces only deformation – a so-called "free temperature bending (FTB)" – but no any stress. Hence, to correlate stresses with the values of temperature gradients, as it is often practiced in the literature, is not correct. Significant are the maximum deviations of the temperature field from linearity, i.e. from FTB. An approximation of the normal stress σ caused by the curvature (non-linearity) of a temperature distribution along a given coordinate x is obtained by [57]:

$$\sigma \approx \alpha_T E \frac{\partial^2 T}{\partial x^2} \quad L^2 \approx \alpha_T E \delta T_{\max} \quad (6.4)$$

with α_T – linear thermal expansion, E – Young's modulus, and L – characteristic length, and δT_{max} – maximum deviation from FTB along a given length. The acting shear stress τ can be deduced from σ by the relation $\tau = f_s\,\sigma$ with f_s the Schmidt factor [55]. For instance, taking the material parameters of silicon near the melting point ($\alpha_T = 4.5 \times 10^{-6}$ K^{-1}, $E = 15 \times 10^4$ MPa) a deviation of $\delta T_{max} = 10$ K generates a normal stress of 6.8 MPa only just below the CRSS of 9 MPa (section 6.1). Much more critical becomes the situation in CdTe ($\alpha_T = 6 \times 10^{-6}$ K^{-1}, $E = 5.2 \times 10^4$ MPa) where already a deviation of 1 K from linearity generates a stress near CRSS (0.2 MPa; see also section 6.1).

However, Indenbom showed also that a free temperature bending without stress is not exclusively correlated with a linear temperature field, but in dependency on the body geometry there are further theoretical solutions possible. For instance, in a ribbon with T-independent height z a stress-free FTB is also presented when $\partial^2 T/\partial x^2 + \partial^2 T/\partial y^2 = 0$. In other words, this condition is fulfilled in each T-field being approximated by the sum of harmonic polynoms [57].

For quantitative estimation of the stress-induced dislocation density until today mostly the viscoplastic model of Alexander–Haasen (AH) is applied [58]. It uses the constitutive law that relates the time-dependent inelastic strain with dislocation density. The plastic shear rate $d\varepsilon_{pl}/dt$ and mobile dislocation density rate $d\rho_{dis}/dt$ are given as

$$
\begin{aligned}
d\varepsilon_{pl} / dt &= \phi\rho_{dis} b v = \phi\rho_{dis} b B_o \tau_{eff}^{m} \exp(-Q/kT) \\
d\rho_{dis} / dt &= K\rho_{dis} v = K\rho_{dis} B_o \tau_{eff}^{m+1} \exp(-Q/kT)
\end{aligned}
\qquad (6.5a,b)
$$

with ρ_{dis} – starting mobile dislocation density, b – Burgers vector, ϕ – geometrical factor relating the direction of the shear strain within the slip system, K – multiplication constant determined from degree of deformation, v – dislocation multiplication rate, B_o – pre-exponential factor, m – material constant, Q – Peierls potential, $\tau_{eff} = \left(\tau - A\sqrt{\rho_{dis}}\right)$ – the effective shear stress on dislocations with A the strain hardening factor = $Gb/[2\pi(1-\nu)]$. For a profound review see [59].

Such quantitative analyses give a good overview on expected value and distribution of dislocation densities according to acting stresses within a growing crystal (Fig. 8). Today, there is an enormous number of publications presenting the stress-dislocation situation in numerous semiconductor and dielectric crystals grown by diverse methods from melt, solution and vapor. One of the noticeable results is that the starting dislocation density is of much lower relevance than the acting stress value. Already after a relative short time period a nearly identical maximum dislocation density is obtained.

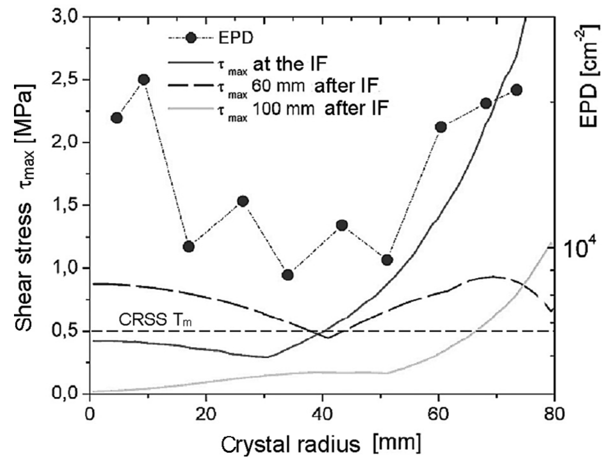

Fig. 8. Correlation between simulated maximum thermo-mechanical shear stress component along the radius of a growing 6 inch GaAs VCz crystal at different distances from the melt–solid interface (IF) and measured etch pit density (EPD) in the as-grown state. The correlation with stress distribution immediately behind the IF is obvious (reported by Ch. Frank-Rotsch and P. Rudolph at the Numeric Meeting of German Ass. of Crystal Growth, November 03–04, 2005).

However, the AH model proves to be not yet perfect. Miyazaki summarizes some necessary modifications such as consideration of different dislocation types, dislocation annihilation and immobilization [59]. The viscoplastic model even fails when considering topological aspects of dislocations like bending and loop formations, for example. Also the interplay with point defects, i.e. dislocation climb, is not considered in the AH model [60]. Totally new mathematical concepts are required when the 3D dislocation dynamics, such as bunching and network generation, needs to be described numerically [61] (see section 6.2).

In summary the cardinal question is generally still open whether it is possible to obtain dislocation-free bulk crystals apart from silicon and germanium. By using dislocation-free seeds the answer lies in Indenbom's theoretical concept whereupon it could be realized at nearly homogeneous temperature fields but also curved ones when they are approximable by a sum of harmonic polynoms (see above). Of course, this proves to be of considerable experimental challenge and could be only solved by applying highly modern temperature controlling systems such as *model-based automation* of each step of the whole crystal growth process [62].

6.3. Dislocation dynamics

6.3.1. Cell patterning

As crystalline solids deform plastically, the expansion of slipped areas leads to an increase in the dislocation line length within the crystal (“dislocation multiplication”). This proliferation of dislocations goes along with their spatial re-distribution and often the formation of heterogeneous *dislocation patterns* in the form of a cellular structure [61]. This can be revealed in most monocrystals and occasionally in epitaxial layers too. There is an increasing need for clarification of such features in semiconductors and dielectric crystals because they markedly influence the device quality such as mesoscopic resistivity variation, charge-transport nonuniformities and impairment of optical transparency.

Principally, dislocations are metastable defects with high energy; their density cannot be drawn from equilibrium thermodynamics, as in case of point defects (see section 3). The thermomechanical work done during plastic flow is mainly dissipated into heat and the rest is stored in the form of elastic dislocation energy. Such process is far from thermodynamic equilibrium and promotes spontaneous forms of self-organization, i.e. *dissipative structures*, such as periodic and cellular dislocation patterns [59] (Fig. 9a–f).

Dislocation networks are observed in crystals independently by which method of phase transition they have been grown [50]. 3D IR laser scattering analysis of as-grown GaAs crystals showed [63] that such dislocation cells are of almost globular shape with nearly dislocation-free interior. In ensemble a configuration of minimum energy is formed. Grange et al. [64] demonstrated by real time X-ray tomography on crystallizing aluminum foils that such cellular patterning takes place only few millimeters behind the propagating solid–melt interface. Thus,

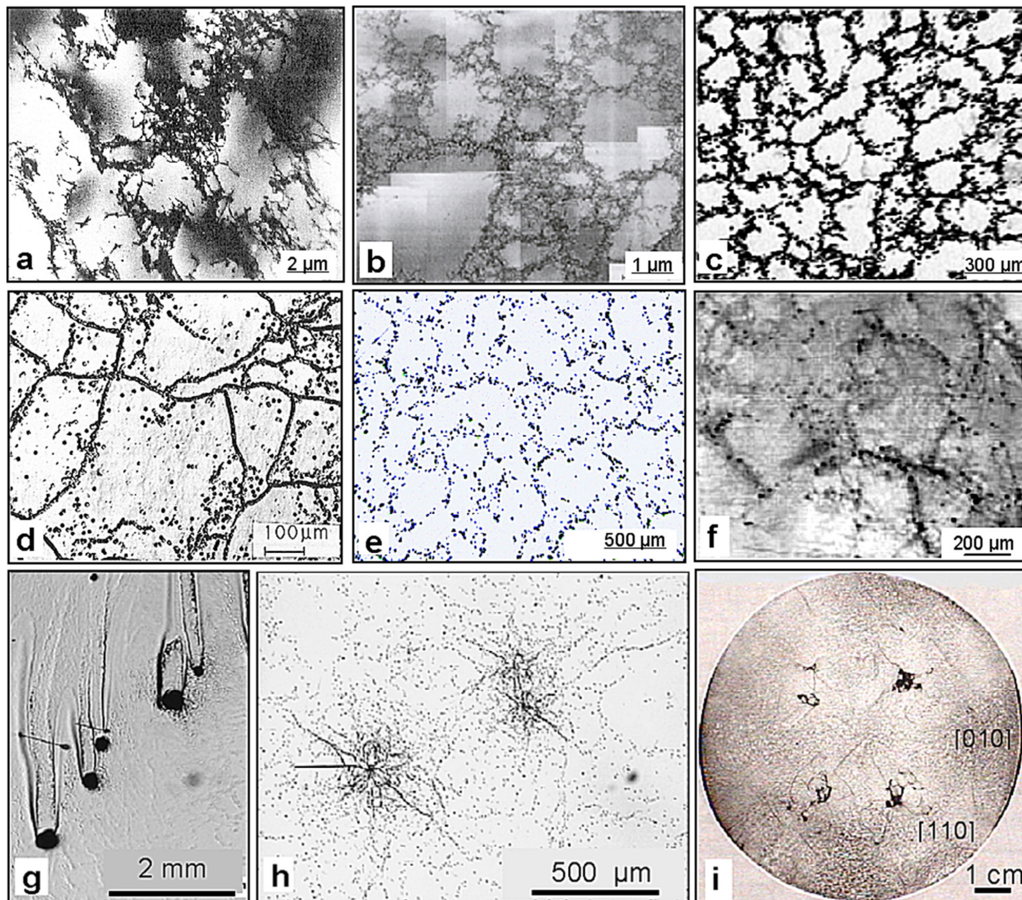

Fig. 9. Dislocation patterns and bunches formed in various crystals under differing load and growth conditions. (a) Mo 12% deformed at 493 K; (b) Cu–Mn crystal deformed at 68.2 MPa; (c) GaAs crystal grown by VCz; (d) CdTe crystal grown by VB; (e) mc-Si grown by VGF; (f) SiC crystal grown by sublimation; (g) dislocation clustering around Ga inclusions in a LEC GaAs crystal; (h) dislocation bundles in directionally solidified mc-Si; (i) dislocation accumulations in concave interface regions in a LEC GaAs crystal (a–f: partially adapted from ref. [50]; g–i: images by U. Juda, IKZ Berlin).

besides high temperature the spatial patterning character requires 3D-type dislocation movements, i.e. climb and cross glide. This has been confirmed by 3D numeric simulations very obviously [65]. It was also shown experimentally that by near-stoichiometric growth of GaAs crystals the markedly decreased native point defect content restrains cellular structures [66]. In other words, each crystallization process with stored dislocations and excess of point defects is escorted by a highly activated dislocation dynamics. At high temperatures the enhanced diffusivity of point defects makes climb a comparable mobility partner of glide.

In addition to high-temperature climb processes, dislocation dynamics (DD) is based on long- and short-range interaction forces such as annihilation and accumulation in walls, as well as dipole and junction formations, respectively [67]. All these processes cause the reduction of the crystal enthalpy. In particular, at the long-range-driven arrangement of dislocations in walls (i.e. cell mantles) the energy gain of each dislocation amounts to ~25%.

Ascertaining the mean cell diameter thanks to the rules of correspondence [51] we are able to estimate the mean dislocation density and value of acting thermomechanical stress (Fig. 10). At first, after Holt's relation (Fig. 10 bottom) $\rho_{dis}^{1/2} \approx \kappa\, d$ (d – cell diameter, ρ_{dis} – dislocation density, κ – factor of proportionality) there is a correlation between cell size and dislocation content. According to the rule of Kuhlmann-Wilsdorf (top Fig. 10) $d = \kappa\, G\, b\, \tau^{-1}$ (G – shear modulus, b – Burgers vector, τ – shear stress) the mean cell diameter depends on the acting stress τ. Finally, Taylor's rule $\tau = \kappa\, G\, b\, \rho_{dis}^{1/2}$ shows the relation between stress and expected dislocation density. These relations have been determined by load investigations of many materials, mainly metals [68] (note, until today, there is still a certain ambiguity concerning the κ factor amounting in the literature between 7 and 20). The author's team found out a near similar behavior in as-grown semiconductor crystals by using $\kappa = 10$ [69]. From these relations follows that substructures should be damped by adherence of lowest as possible thermomechanical stress during growth. Additionally, solution hardening by doping in order to increase the critical resolved shear stress proves to be helpful [50]. Finally, in compounds the control of stoichiometry reduces the intrinsic point content, and thus also the climb probability [66].

It is noteworthy that one has to differ between the above discussed cell type, originated by DD, and small-angle grain boundaries generated by dynamic polygonization (section 7), as well as by a cellular interface shape due to morphological instability caused by

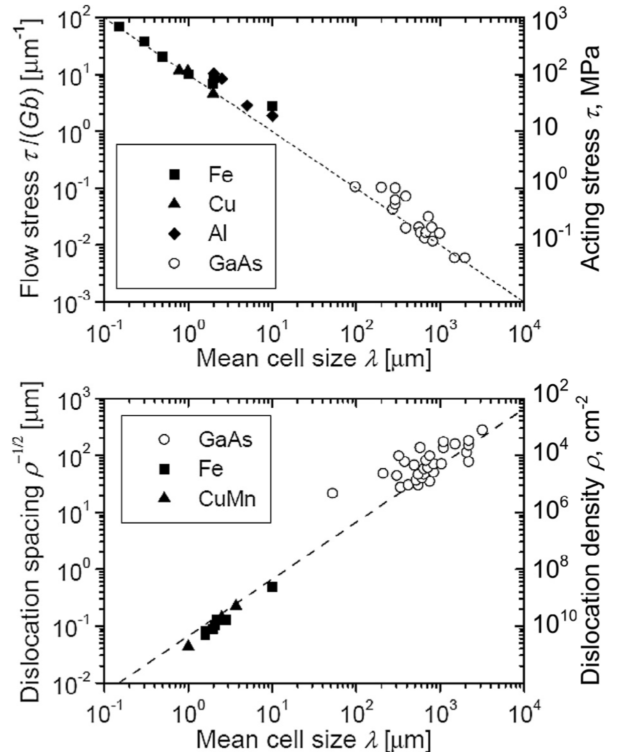

Fig. 10. Scaling of dislocation cell patterns in metals and semiconductors. Top figure: cell size vs. flow stress (relation of Kuhlmann-Wilsdorf). Bottom figure: cell size vs. mean dislocation spacing and density (relation of Holt; adapted from refs. [50,51]).

constitutional supercooling (section 5.4). As it was demonstrated by real-time synchrotron x-ray topography on Al–Cu alloys [70] a cellular interface shape is able to redirect and collect growing-in dislocations along the grooves between the cell lamellae appearing in cross sectional cuts as small-angle grain structure too. An effective mixing measure of the fluid phase is required to prevent such harmful morphological instability (section 5.4).

Finally, well-patterned misfit dislocations, the so-called "cross hatches," are generated in epitaxial systems where a marked difference between the lattice constants of the growing layer a_l and substrate a_s does exists, i.e. $f = (a_l - a_s)/a_s > 3\%$. After a critical height h_c the strained pseudomorphology is overcame by introduction of alternating edge dislocations with periodicity $\lambda \sim b/f$ (b – Burgers vector) showing dislocation lines parallel to the substrate plane, i.e. in lateral direction.

6.3.2. Dislocation bunching and inclination

The appearance of bunched dislocations (often named "clusters") is reported in many single crystalline materials including directionally solidified polycrystals, like

in multicrystalline (mc) silicon ingots. Once they are formed they follow mostly the propagating solidification interface through the whole crystal remembering *veins* (Fig. 9g–i).

Principally, one has to differ between two types of bunching – (i) originated around foreign particle inclusions (Fig. 9g), and (ii) consisting of a high number of tangled dislocations without any core of second phase (Fig. 9h–i). Type (i) is today well understood. For instance, during the growth of compounds without stoichiometry control, the excess component is incorporated as liquid inclusions mostly generating marked misfit stress during solidification at the boundary to the matrix. As a result, a halo of high dislocation density is formed around the inclusion (see section 8). Due to the traveling solvent mechanisms the included micro droplets penetrate against the acting temperature gradient by releasing a trail with bunched misfit dislocations (Fig. 9g).

More complex proves to be the defect nature of type (ii). It seems to be of statistical appearance. Recently Kubin [61] pointed out that in materials under strain the plastic flow is not uniform at a fine scale. The inhomogeneous release of elastic energy gives rise to the emission of *acoustic waves* (avalanches) interplaying with stored sessile dislocations and micro obstacles (precipitates, vacancy condensations). In the course of cooling down sporadic clouded dislocation patterns are frozen in.

However, also a correlation of clustering with the propagating interface morphology is observed. For instance, growing-in dislocations are accumulated within concave regions or grooves. Even cellular phase boundaries with re-entrant corners appear at multi-grain growth or constitutional supercooling (section 5.4). As a result, the dislocations are bended following normally the growth face inclination at the cell flanks. Such characteristic behavior has been explained by Klapper using the minimum-energy or zero-force theorems [71] but it can be also treated in the sense of image dislocation (section 6.1; see Fig. 7). Further, a characteristic build-up at the concave-to-convex transition region has obviously to do with collision of dislocation glides along the basic glide system [72]. Once clusters are formed they follow the propagating interface through the whole crystal.

To avoid dislocation bunching a convex interface curvature without concave parts and grain boundaries is of advantage. However, to damp the danger of thermo-mechanical stress generation such an interface course should be convex curved as minimum as possible (see also section 6.2). Further, the incorporation of high stress inducing inclusions must be prevented.

On the other hand, the follow-up of dislocations normally to the interface is of highest practical importance for their inclination, and therefore reduction in the course of *epitaxial processes*. As it is well known apart from misfit dislocations being concentrated at the substrate–layer interface region (section 6.3.2) there are threading dislocations with lines normally directed to the growing layer surface. At last, they determine the dislocation density of the as-grown layer, and thus its quality used for device production. One of the counteracting measures is to reduce the dislocations by a *two-step growth mode*. First, after a seed film at relatively low-temperature a nucleation layer consisting of 3D micropyramids is grown. Due to the shaping of the micro pyramids by energetically minimized facets the threading dislocations are bent via these boundary surfaces toward the lateral direction [49]. Then the temperature is enhanced and a lateral 2D layer-by-layer overgrowth takes place supporting the lateral outgrowth of dislocations. Such 3D–2D transition is also controlled by the V/III ratio in the vapor phase as reported at MOVPE growth of GaN layers on sapphire substrate (e.g. [73]). The two-step growth is also used for obtainment of GaAs layers on silicon substrates (e.g. [74]).

As was mentioned in section 6.1 a dislocation inclination can be also achieved by desymmetrization of the local stress field around dislocations with the aid of certain doping elements. For instance, according the μ-PL analysis of Forghani et al. [47] a favorable bending has been observed in Si-doped GaN crystals obviously caused by formation of asymmetric strain dipoles with reduced compressive pole around dislocation lines.

6.3.3. Reduction of misfit dislocations at epitaxy

One of the major targets of the crystal grower is to reduce the misfit stress at heteroepitaxial processes that generates system bowing and dislocations. One possibility is the discretization of the surface profile of the substrate by a so-called "*surface structuring or texturing*." By means of structural etching or masking various profiles can be obtained such as parallel equidistant strips or honeycomb grid patterns made of hillocks or truncated cones ("Kagome" structures). Even a "simple" surface roughening is used. For instance, the dislocation penetration points across the substrate surface show mostly enhanced etching ability usable for making a porous surface morphology.

The basic idea is to minimize the mechanical contact between substrate surface and epitaxial layer. As has been shown theoretically markedly dislocation-reduced growth is obtained on small seed pads directed along a distinct crystallographic orientation [75]. The critical film thickness (still without misfit dislocations) rises sharply when the above strip or knob plane is sufficient small. Thus,

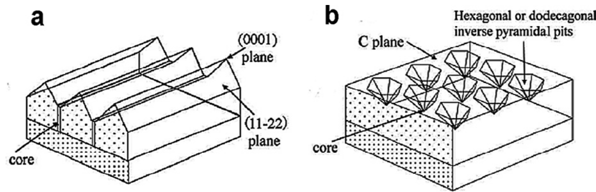

Fig. 11. GaN heteroepitaxy on patterned substrates on (a) stripe-shaped patterned template and (b) dot-type core (adapted from ref. [52]).

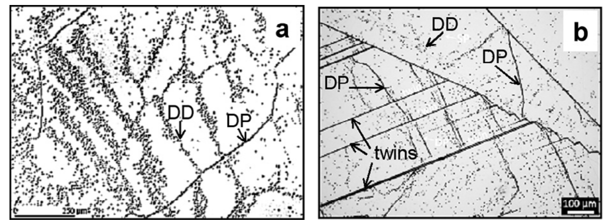

Fig. 12. Low-angle grain boundaries in (a) Czochralski-grown CaF_2 crystal (image from U. Juda, IKZ) and (b) directionally solidified mc-Si ingot (image from T. Evrik, Univ. Trondheim). DD – cell walls obtained by high-temperature dislocation dynamics combining glide with point-defect assisted claim; DP – grain boundaries obtained by dynamic polygonization.

the coalescing layers retain this condition during overgrowing the seeded strips or hillocks. As related growth techniques the epitaxial lateral overgrowth (ELOG) [76] and facet-assisted epitaxial lateral overgrowth (FACELO) [49,77] have to be successfully applied for growth of GaN, SiC, InP, etc. layers on various substrates (Fig. 11). The acting stress (i.e. the system bowing) and, thus, threading dislocation density was considerably decreased [52].

Further methods for stress decoupling between substrate and epitaxial layer are buffer films made of nanowires, graphenes or compositionally graded buffer layers.

7. Grain boundaries, facets and twins

7.1. Low- and large-angle grain boundaries

A grain boundary is the interface between two nearly perfectly built structure regions in solid materials. One has to distinguish between low-angle grain boundaries with tilt angles θ in the region of arcsec–arcmin and large-angle grain boundaries with tilts of some degrees. The value of θ can be determined by the distance d of etch pits arranged in rows along the grain boundaries ($\sin\theta = b/d$ [rad] with b – Burgers vector) and by the full width of half maximum (FWHM) of the X-ray Rocking curve, for example. Grain boundaries are of enhanced energy γ increasing with θ as $d\gamma/d\theta > 0$ until about 11–15°. At higher disorientations this dependence is vanishing and becomes $d\gamma/d\theta \approx 0$. Among the material scientists this moment is often named as transition from single to polycrystallinity.

The origins of *low-angle grain boundaries* are (i) dynamic polygonization (DP) in the course of plastic relaxation due to thermomechanical stress, (ii) high-temperature dislocation dynamics (DD) combining glide with point-defect assisted claim (treated in section 6.3.1), and (iii) morphological instability of the melt–solid interface in the form of cellular interface shape (treated in section 5.4). The driving force of DP is the enthalpy minimization by dislocation annihilation and lining up of the excess dislocations in low-angle grain boundaries (named geometrically necessary dislocations – GND). In such wall arrangement the energy of single dislocation is reduced of about 75%. As a result the crystal structure is plastically released by generation of a network of cells with sharp walls consisting of a single row of dislocations with identical Burgers vector. Compared to that in case (ii) the phenomenon of dissipative structuring (see section 6.3.1) plays a decisional role. A small-angle globular cellular structure is formed by the interplay between cross glide and climb, i.e. under participation of the intrinsic point defect diffusivity. In this process the cell walls are typically tangled and mostly of lower tilt than in case (ii) [50]. Often both types of cell structures are observed together whereas the DP cell interiors consist of DD subcells as in unidirectionally solidified mc-silicon ingots (Fig. 12).

Low-angle grain boundaries prove to be also a serious problem in epitaxial processes. Especially, at vapor growth of GaN layers on various substrates the coarsening of primarily nucleated GaN islands generates a marked tensile stress as was explained by Nix and Clemens [78]. Due to the elastic displacement between the islands a biaxial strain is formed enhancing the bowing and even cracking of the growing layer. It was observed that high-mobility ad-atoms can help to relax such stress by their diffusion into the gaps between. However, a rapid lateral overgrowth mode would be of more efficiency.

Large-angle grain structures are well known from multinucleated crystallization such as metallurgical casting. With increasing importance of directional solidification of multicrystalline (mc) silicon ingots for photovoltaics (PV) also in semiconductor industry, the control of large-angle grain growth comes to the fore. However, apart from the reduced material cost, such grains formed by spontaneous nucleation at the container bottom may degrade the solar cell efficiency, especially when a high density of dislocations and impurities are captured upon. Many experiments have been provided to practice the grain coarsening on the basis of Gibbs–Thomson effect

whereupon grains of small dimension disappear due to their heightened chemical potential compared to the larger ones. Nowadays, the nucleation step is controlled to obtain a small but uniform grain size being constant during the whole ingot height. It has been observed that the density of dislocation clusters is much lower in such structure. Due to the relatively high solar cell efficiency (>18%) of wafers from such ingots, this crystallization technology was recently introduced as "high-performance mc-Si" [79].

Of course, in the field of single crystalline growth the cardinal aim is to prevent large-angle grain structures impairing the favorable anisotropic, electronic and optical qualities of monocrystals. As it is well known, one of the first tasks of the pioneering works was the insertion of a seed crystal into the solution tanks, a dipping into the melt or grain selection by container necking. Additionally, to guarantee a grain-free growth the thermomechanical stress must be reduced to a lowest possible minimum. The growing out of grains is enhanced by slightly convex curved crystallization fronts. Dissipative cellular substructures can be avoided by minimization of intrinsic point defects (near stoichiometric growth conditions) and solution hardening.

7.2. Facets and twins

High-purity and high-quality crystals tend in low temperature gradients to assume polyhedral shape composed of atomically smooth planes – named *facets* – with lowest free surface energy. Also at growth methods under low absolute temperatures, like from aqueous solutions and vapor, this tendency is very pronounced. Frankly spoken, such occurrence cannot be attributed to a defect structure. However, when both atomically smooth and rough planes are presented at the same time, critical situations can appear. This is the case at melt growth of semiconductors with diamond (Si, Ge) and zincblende structure (GaAs, InP, CdTe, etc.) having {111} smooth planes. At an <111 > growth orientation from melt with convex interface a $(\bar{1}\bar{1}\bar{1})$ facet appears in the center. Due to its requirement of higher supercooling compared to the surrounding region and, therefore, discontinuous lateral growth kinetics impurities and dopants are here incorporated with much higher concentration than outside the facet region. As a result a dramatic radial chemical inhomogeneity with enriched core region occurred not more describable by equilibrium effective segregation coefficient (for more details see refs. [1,4]). On the other hand, during crystal pulling with convex interface along <100>-orientation the four {111} facets appear at the periphery and may affect the meniscus stability and even the diameter control algorithm.

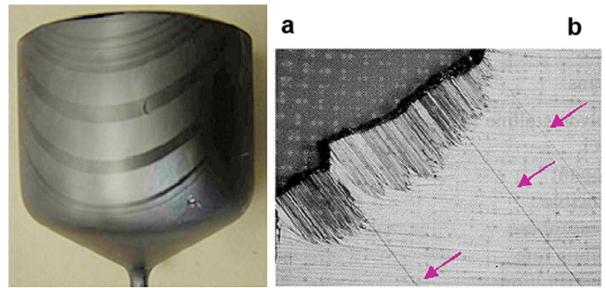

Fig. 13. Twinning in InP crystals. (a) 4 inch VGF InP crystal with numerous twins (adapted from ref. [23]; (b) twin generation at {111} facets within the shoulder region of an LEC InP crystal (adapted from ref. [80]).

Of course, all above mentioned facts are completely transferable to oxide crystal growth too where faceting is much more pronounced due to the higher bond energies. Moreover, due to the enhanced share of radiation often the heat is considerably back-reflected at formed facets. Especially when they inclined toward the melt level the isotherm isotropy around the growing crystal can be disturbed.

As has been observed in many Czochralski and Bridgman experiments *growing-in twins* are closely correlated with the presence of {111} facets at the periphery of propagating interfaces (Fig. 13). In the diamond and zincblende structures, twinning is specified by a rotation of the lattice by 60° about a < 111 > axis, the twin lying even on the orthogonal {111} plane. Voronkov [81] found out that because of the orientation dependence of interfacial energies in the presence of facets, there is a configuration of the 3-phase boundary for which, for sufficiently large supercooling, the free energy of formation of a critical nucleus is actually lowered by forming that nucleus at the 3-phase boundary in twinned orientation, whereupon the highest danger of twinning exists in materials with high ionicity showing the lowest stacking fault energies [82]. In fact, InP and CdTe with degrees of ionicity of 42% and 72% and stacking fault energies of 18 and 11×10^{-7} J cm^{-2}, respectively, show an extremely high twinning statistics among the semiconductor compounds. Hurle [83] has provided a possible thermodynamic description, which shows that a twinned nucleus is favored if the supercooling exceeds the critical value

$$\delta T^* = (\gamma T_m / h\Delta H_{SL}) A^* \quad (7.1)$$

with γ being the twin plane energy (~stacking fault energy), T_m melting temperature, h the nucleus height,

ΔH_{SL} the latent heat of fusion, and A^* the reduced work of formation of a nucleus intersecting the 3-phase boundary. Indeed an enhanced twin probability was observed on large facets being equitable with high supercooling [80]. Further Hurle pointed out that twinning will especially occur if a critical angle of conical growth presenting a portion of crystal surface normal to <111 > is sampled during the growth. In fact, as was recently repeatedly demonstrated [84], twin-free InP crystal can be grown by large cone angle, nearly 75–90°. But in agreement with many former experiments the results were not unambiguous. According to the still high statistical rate the authors conclude that the stability of the growth system plays the dominant role and deserves more attention than the research for the cone angle. This is in agreement with Neubert et al. [85], which summarized the following precondition for minimization of twinning probability: due to the direct correlation of twin formation frequency with high growth rates and large growth rate fluctuations, the growth system should be stabilized by directly damping the thermally or mechanically induced growth rate fluctuations down due to (i) reduction of melt convection (hot zone design, magnetic fields, etc.) and (ii) precise feedback control of crystal shape and growth rate.

8. Foreign particles

The presence of micro-particles of foreign phases (second phases) or microvoids (bubbles) within the matrix of many single crystals is a long-term object of research due to their harmful character. Micro-particles impact the optical transmission, electrical carrier life and structural perfection. They are sites of misfit stress, and thus of dislocation generation and bunching around their periphery. Further, they are sources of out-diffusing of embedded impurities. Microvoids affect the wafer quality for epitaxial processes onto them. This has proven a particular problem in silicon wafers taken from crystals grown at economically favored high growth rate (see section 5.1). The following are two main different origins of their generation:

(i) native *point defect condensation* leads during cooling to the nucleation of *precipitates* or microvoids via interstitial or vacancy agglomeration, respectively, and
(ii) *incorporation* in favorable sites along the propagating crystallization front named *inclusions*.

Usually both kinds of foreign phases differ by their size. Whereas precipitates show characteristic dimensions in the range of 10–1000 nm, inclusions are typically of diameters >1 μm [86]. This classification, however, is approximated only and cannot serve as exact criterion of distinction. The size of both kinds of microparticles or voids depends on various parameters like concentration ratio of the components, degree of supersaturation, interface instabilities, as well as on growth and cooling rates which markedly influence the ripening time and extent. Nevertheless, their origins are different and should be always distinguished [87].

The condensation of native point defects in the form of precipitates and microvoids is caused by their decreasing solubility in the course of the crystal cooling. Even in non-stoichiometric compound crystals, the retrograde solidus course of the existence region produces precipitates of the excess component. In comparison, inclusions are incorporated at the growing interface mostly as melt-solution droplets separated from the diffusion boundary layer and gas bubbles often generated by dissociation of volatile compounds in the fluid phase. During the crystal cooling the droplets solidify at the eutectic point generating high misfit stress and dislocations. Their presence increases with conditions of morphological instability (section 5.4). Indeed, Henager et al. [88] correlated the distribution appearance of inclusions in (Cd, Zn)Te crystals grown from Te-rich melt-solution with constitutional supercooling. The often observed Te inclusion arrangement in the form of pearl-strings was attributed to the Rayleigh–Plateau instability.

Favored sites of precipitate ripening are dislocations, as has been concluded from LST analysis in GaAs [89], for example. In dependency on the deviation from stoichiometry in semiconductor and dielectric compound crystals, average precipitate densities in the region of 10^8–10^{12} cm^{-3} have been ascertained. Some papers reported that half-empty precipitates revealed by high-resolution transmission electron microscopy obviously were caused by vacancy condensation on one of the sublattices accompanied by conglomeration of excess atoms of the opposite sublattice.

Preferred sites of inclusion incorporation are reentrant angles of grain boundaries, grooves of cellular interfaces and twin lamellae crossing the interface. Mostly they also consist of an excess component in non-stoichiometric crystals due to their enrichment in the diffusion boundary layer. Thus, a slightly axial increase of their density along the growth direction is reported [86] due to the segregation via excess component. Non-stoichiometric melt-solution inclusions show a specific crystallization genesis within the already solidified matrix [86]. Often they are embedded in a negative polyhedron formed by adjacent planes of the crystal matrix.

Whereas the incorporation of a melt-solution droplet of constituents immediately from a markedly enriched

diffusion boundary layer can be assumed to be energetically facilitated in case of foreign particles and gas bubbles, a hydrodynamic splitting pressure of repulsive force is acting at the interface. Chernov and Temkin [90] described this effect in detail and found out that the overgrowth probability increases with decreasing particle/ bubble diameter, increasing growth velocity and decreasing temperature gradient. For continuous growth the critical interface velocity v^* depends on the particle radius R as [90]

$$v^* = 0.11(B_3 / \eta R)(2\gamma / B_3 R)^{1/3} \tag{8.1}$$

with B_3 the constant of disjoining pressure, η the dynamic viscosity of the melt, and γ the interface energy between solid and melt.

Indeed, the experimental tests of Fedorov [91] with Ni particles of diameters between 25 and 150 µm in salol showed that there is a repulsive effect when the velocity is chosen undercritically (Fig. 14). As it was also demonstrated the repulsion differs on various facets.

Such studies are also helpful for minimization of SiC and Si_3N_4 particle incorporation in directionally solidified silicon ingots for use in photovoltaics. Such second phases are nucleated when the enriched concentration within the diffusion boundary layer of always presented carbon and nitrogen exceeds the solubility of C and N in Si melt being for both about 5×10^{18} cm^{-3}. Recent phase-field simulations of SiC particle capture at directional solidification of silicon and comparison with first experiments show that even the particle morphology can have a larger effect on the critical growth velocity [92].

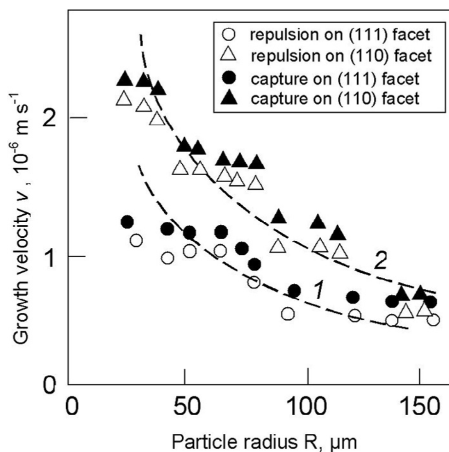

Fig. 14. Repulsion and capture of Ni particles on (111) and (110) facets at growing melt–solid interface of salol crystals. Curve 1 – Eq. (8.1) taking $B_3 = 10^{-20}$ J [90]; curve 2 – taking the facet velocity ratio $v^*_{111}/v^*_{110} = \cos\varphi = 0.55$ (adapted from ref. [91]).

It is obvious that during the cooling down process foreign particles within a crystalline matrix induce mechanical stress due to their differing crystallographic structure and thermal expansion. The situation is more critical when first liquid droplets with inner pressure are presented, which during cooling down crystallize and the volume is enlarged by in-diffusion of an excess component. It was shown by phase-field simulations [93] that in dependency on size, morphology, concentration and share of inner voids, Te precipitates generate a strain in the range of 0.2–0.7 GPa quite enough to act as micro obstacles for dislocation dynamics, and therefore clouded dislocation patterning (see section 6.3.2).

Yadava et al. [94] attributed the often observed characteristic star-like dislocation bunching around Te inclusions to the Greenwood–Foreman–Rimmer mechanism (Fig. 15). Therefore the generation of interstitial dislocation loops takes place when the excess droplet pressure p' acting toward the surrounding matrix produces shear strain in the neighboring solid region, which above a threshold level punches a part of an atomic layer and places it as a platelet of the interstitials sandwiched between two adjacent regular atomic planes. Such loop punching along energetically most favorable atomic planes will occur if [94]

$$p' = p - \frac{2\gamma_{IF}}{r_d} \geq \frac{G_m b}{2\pi r_d} \ln\left(\frac{r_d}{b}\right) \tag{8.2}$$

where p is the internal droplet pressure, γ_{IF} is the liquid (Te)–solid (CdTe) interface energy, r_d is the droplet radius, b is the Burgers vector of the dislocation loop, and G_m the shear modulus of the matrix. Thus, apart from γ_{IF} decisional significance becomes p depending on liquid droplet density, liquid association energy and temperature (for more details see ref. [91]).

Generally, the precipitate density is minimized at growth under stoichiometric conditions or/and by after annealing in vapor of volatile component. As we demonstrated [27], on applying the VCz growth of GaAs without boric oxide encapsulant, Ga-rich melt compositions of mole fraction of $x_L \leq 0.45$ yield near-stoichiometric crystals essentially free of precipitates. Oda et al. [30] developed a multi-stage post-growth *wafer annealing* technology for semi-insulating GaAs. Highly uniform substrates with markedly decreased arsenic precipitate density were obtained. Subsequently, post-growth bulk and wafer annealing has been very successfully used for quality improvement of many materials.

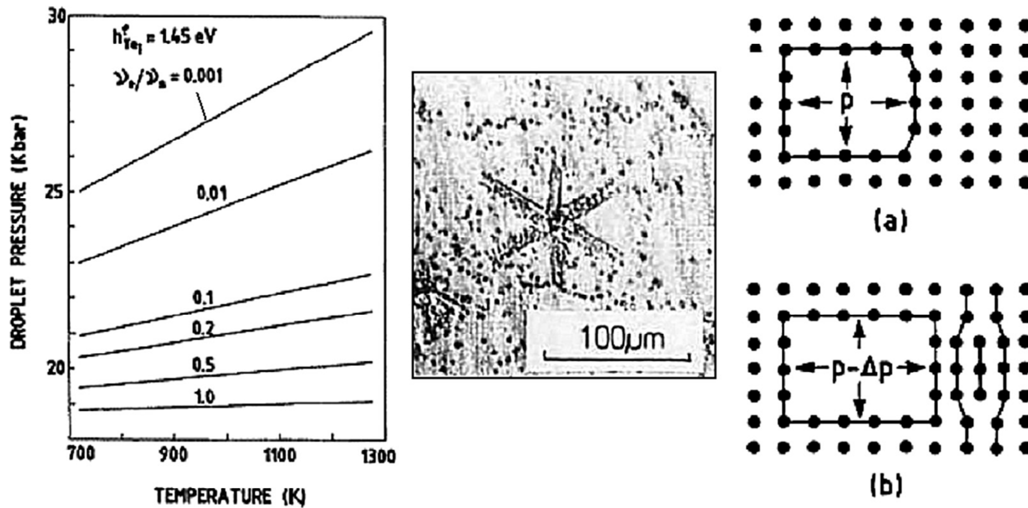

Fig. 15. Star-like dislocation generation around Te inclusion in CdTe crystals. Left – theoretical variation of Te droplet pressure with temperature for different liquid-to-solid vibrational frequency ratios $\nu_l/\nu_s = 1 - 0.001$ under fast cooling (h^f_{Te} – Te interstitial formation energy); middle – prismatic dislocation loop punching around Te inclusion revealed by etch pits; right – schematic illustration of Greenwood–Foreman–Rimmer mechanism of interstitial dislocation loop punching before (above) and after (below) a loop is formed (adapted from ref. [92]).

The incorporation of inclusions can be prevented by (i) growth from the congruent melting point, (ii) choice of undercritical growth velocities, and (iii) reduction of rejected solvent concentration, i.e. diffusion boundary layer, at the interface by proper melt or solution mixing techniques [41].

References

[1] D.T.J. Hurle, P. Rudolph, A brief history of defect formation, segregation, faceting, and twinning in melt-grown semiconductors, in: R.S. Feigelson (Ed.), 50 Years Progress in Crystal Growth, Elsevier, Amsterdam, 2004, pp. 109–124.
[2] P. Rudolph, Fundamentals of defects in crystals, in: M. Skowronski, J.J. DeYoreo, C.A. Wang (Eds.), Perspectives on Inorganic, Organic and Biological Crystal Growth: From Fundamentals to Applications, AIP, Melville, 2007, pp. 69–92. Conference Proc. No 916.
[3] P. Rudolph, Thermodynamics, origin, and control of defects, in: H. Scheel, P. Capper (Eds.), Crystal Growth Technology, Wiley VCH, Weinheim, 2008, pp. 73–102.
[4] P. Rudolph, Defect formation during the crystal growth from melt, in: G. Dhanaraj, K. Byrappa, V. Prasad, M. Dudley (Eds.), Springer Handbook of Crystal Growth, Springer, Heidelberg, 2010, pp. 153–202.
[5] H. Klapper, P. Rudolph, Defect generation and interaction during crystal growth, in: T. Nishinaga, P. Rudolph, T. Kuech (Eds.), Handbook of Crystal Growth, Vol IIB, second ed., Elsevier, Amsterdam, 2015, pp. 1093–1142.
[6] F.A. Kröger, The Chemistry of Imperfect Crystals, North-Holland Publ., Amsterdam, 1964.
[7] I. Prigogine, Non-Equilibrium Thermodynamics of Irreversible Processes, Charles C. Thomas Publ., Springfield, 1955.
[8] Y. Mori, M. Imade, M. Maruyama, M. Yoshimura, H. Yamane, F. Kawamura, et al., T. Nishinaga, P. Rudolph, T. Kuech (Eds.), Handbook of Crystal Growth, Vol IIA, second ed., Elsevier, Amsterdam, 2015, pp. 505–534.
[9] A.F. Ioffe, A.R. Regel, Non-crystalline, amorphous and liquid electronic semiconductors, Prog. Semicond. 4 (1960) 237–291.
[10] P. Moskvin, M. Antonov, G. Olchowik, J.M. Olchowik, A. Zdyb, S. Gulkowski, et al., Polyassociative model of A_2B_6 semiconductor melt and P-T-X phase equilibria in Zn-Cd-Te system, TASK Quarterly, Sci. Bull. Acad. Computer Centre Gdansk 15 (2011) 121–130 and Russ. J. Phys. Chem. 84 (2010) 1832–1837.
[11] J.M. Garcia-Ruiz, F. Otalora, Macromolecular crystals – growth and characterization, in: G. Müller, J.J. Metois, P. Rudolph (Eds.), Crystal Growth – From Fundamentals to Technology, Elsevier, Amsterdam, 2004, pp. 369–390.
[12] A. Moreno, B. Quiroz-García, F. Yokaichiya, V. Stojanoff, P. Rudolph, Protein crystal growth in gels and stationary magnetic fields, Cryst. Res. Technol. 42 (2007) 231–236.
[13] J.-P. Gaspard, J.-Y. Raty, R. Céolin, R. Bellissent, Local orders in II-VI liquid compounds, J. Non Cryst. Solids 205–207 (1996) 75–78.
[14] P. Rudolph, H.J. Koh, N. Schäfer, T. Fukuda, The crystal perfection depends on the superheating of the mother phase too – experimental facts and speculations on the “melt structure” of semiconductor compounds, J. Cryst. Growth 166 (1996) 578–582.
[15] H. Bensalah, J. Crocco, V. Carcelen, A. Black, Q. Zheng, J.L. Plaza, et al., Effect of superheating and fast cooling on Te inclusions of $Cd_{0.9}Zn_{0.1}Te$:In crystals grown by vertical gradient freezing, J. Cryst. Growth 361 (2012) 5–10.
[16] N. Zaitseva, L. Carman, Rapid growth of KDP-type crystals, Prog. Cryst. Growth Charact. Mater. 43 (2001) 1–118.
[17] V.V. Voronkov, Grown-in defects in silicon produced by agglomeration of vacancies and self-interstitials, J. Cryst. Growth 310 (2008) 1307–1314.
[18] J. Friedrich, W. von Ammon, G. Müller, Czochralski growth of silicon crystals, in: T. Nishinaga, P. Rudolph, T. Kuech (Eds.), Handbook of Crystal Growth, Vol IIA, second ed., Elsevier, Amsterdam, 2015, pp. 45–104.

[19] J. Vanhellemont, The *v/G* criterion for defect-free silicon single crystal growth from a melt revisited: implications for large diameter crystals, J. Cryst. Growth 381 (2013) 134–138.
[20] T.Y. Tan, H.-M. You, U.M. Gösele, Thermal equilibrium concentrations and effects of negatively charged Ga vacancies in n-type GaAs, Appl. Phys. A 56 (1993) 249–258.
[21] P. Kempisty, P. Strak, K. Sakowski, S. Krukowski, Adsorption of gallium on GaN(0001) surface in ammonia-rich conditions: a new effect associated with the Fermi level position, J. Cryst. Growth 401 (2014) 78–81.
[22] P. Rudolph, F.M. Kiessling, The horizontal Bridgman method, Cryst. Res. Technol. 23 (1988) 1207–1224.
[23] M. Jurisch, S. Eichler, M. Bruder, Vertical Bridgman growth of binary compound semiconductors, in: T. Nishinaga, P. Rudolph, T. Kuech (Eds.), Handbook of Crystal Growth, Vol IIA, second ed., Elsevier, Amsterdam, 2015, pp. 331–372.
[24] P. Rudolph, Fundamental studies on Bridgman growth of CdTe, Prog. Cryst. Growth Charact. Mater. 29 (1995) 275–381.
[25] F.M. Kiessling, Characterization and control of defects in VCz GaAs crystals grown without B_2O_3 encapsulant, in: P. Capper, P. Rudolph (Eds.), Crystal Growth Technology. Semiconductors and Dielectrics, Wiley-VCH, Weinheim, 2010, pp. 75–100.
[26] M. Neubert, P. Rudolph, Growth of semi-insulating GaAs crystals in low temperature gradients by using the vapour pressure controlled Czochralski method (VCz), Prog. Cryst. Growth Charact. Mater. 43 (2001) 119–185.
[27] F.-M. Kiessling, P. Rudolph, M. Neubert, U. Juda, M. Naumann, W. Ulrici, Growth of GaAs crystals from Ga-rich melts by the VCz method without liquid encapsulation, J. Cryst. Growth 269 (2004) 218–228.
[28] E. Pfeiffer, P. Rudolph, Verfahren zur Züchtung transparenter oxidischer Einkristalle hoher Brechungszahl nach der Czochralski-Methode, Patent DD 290 226, 1989.
[29] J. Franc, L. Sedivy, E. Belas, M. Bugar, J. Zazvorka, J. Pekarek, et al., Melt growth and post-grown annealing of semiinsulating (CdZn)Te by vertical gradient freeze method, Cryst. Res. Technol. 48 (2013) 214–220.
[30] S. Oda, M. Yamamoto, M. Seiwa, G. Kano, T. Inoue, M. Mori, et al., Defects in and device properties of semi-insulating GaAs, Semicond. Sci. Technol. 7 (1992) A215–A223.
[31] P. Rudolph, Elements of thermodynamics for understanding and design of crystal growth processes, in: R. Fornari, C. Paorici (Eds.), Theoretical and Technological Aspects of Crystal Growth, Trans Tech Publications, Zuerich, 1998, pp. 1–26.
[32] A.G. Ostrogorsky, M.E. Glicksman, Segregation and component distribution, in: T. Nishinaga, P. Rudolph, T. Kuech (Eds.), Handbook of Crystal Growth, Vol IIB, second ed., Elsevier, Amsterdam, 2015, pp. 995–1048.
[33] J.A. Burton, R.C. Prim, W.P. Slichter, The distribution of solute in crystals grown from the melt, J. Chem. Phys. 21 (1953) 1987–1991.
[34] E. Scheil, Bemerkungen zur Schichtkristallbildung, Z. Metallkd. 34 (1942) 70–72.
[35] W.A. Tiller, Principles of solidification, in: J.J. Gilman (Ed.), The Art and Science of Growing Crystals, John Wiley & Sons, New York, 1963.
[36] W.G. Pfann, Zone Melting, John Wiley & Sons, New York, 1958.
[37] O. Madelung, Zur Theorie des Zonenziehens von Halbleitern bei Gegenwart einer Gasphase, Z. Phys. 162 (1961) 508–515.
[38] N. Sato, M. Kakimoto, Y. Kadota, The carbon and boron concentration control in GaAs crystals grown by liquid encapsulated Czochralski method, in: A. Milnes, C.J. Miner (Eds.), Semi-Insulating III-V Materials, Adam Hilger, Toronto, 1990, pp. 212–218.
[39] S. Eichler, A. Seidl, F. Börner, U. Kretzer, B. Weinert, A combined carbon and oxygen segregation model for the LEC growth of SI GaAs, J. Cryst. Growth 247 (2003) 69–76.
[40] D.T.J. Hurle, E. Jakeman, Effect of solutal convection on the morphological stability of a binary alloy crystal, J. Cryst. Growth 58 (1982) 163–179.
[41] P. Rudolph, K. Kakimoto, Crystal growth from melt under external force fields, MRS Bull. 34 (2009) 251–258.
[42] W.A. Tiller, K.A. Jackson, J.W. Rutter, B. Chalmers, Acta Metallurg. 1 (1953) 428–437.
[43] W.W. Mullins, R.F. Sekerka, Stability of planar interface during solidification of a dilute alloy, J. Appl. Phys. 35 (1964) 444–451.
[44] J. Frenkel, Zur Theorie der Elastizitätsgrenze und der Festigkeit kristallinischer Körper, Z. Phys. 37 (1926) 572–609.
[45] S. Brochard, J. Rabier, J. Grilhe, Nucleation of partial dislocations from a surface-step in semiconductors: a first approach of the mobility effect, Eur. Phys. J. Appl. Phys. 2 (1998) 99–105.
[46] M. Soleymani, M.H. Parsa, H. Mirzadeh, Molecular dynamics simulation of stress field around edge dislocations in aluminum, Comput. Mater. Sci. 84 (2014) 83–96.
[47] K. Forghani, L. Schade, U.T. Schwarz, F. Lipski, O. Klein, U. Kaiser, et al., Strain and defects in Si-doped (Al)GaN epitaxial layers, J. Appl. Phys. 112 (2012) 093102.
[48] M. Tang, G. Xu, W. Cai, V. Bulatov, Dislocation image stresses at free surfaces by the finite element method, Mater. Res. Soc. Symp. Proc. 795 (2004) U2.4.1–2.4.5.
[49] P. Vennéguès, B. Beaumont, V. Bousquet, M. Vaille, P. Gibart, Reduction mechanisms for defect densities in GaN using one- or two-step epitaxial lateral overgrowth methods, J. Appl. Phys. 87 (2000) 4175–4181.
[50] P. Rudolph, Dislocation patterning in semiconductor compounds, Cryst. Res. Technol. 40 (2005) 7–20.
[51] M. Zaiser, Dislocation patterns in crystalline solids – phenomenology and modeling, in: G. Müller, J.-J. Metois, P. Rudolph (Eds.), Crystal Growth – From Fundamentals to Technology, Elsevier, Amsterdam, 2004, pp. 216–238.
[52] T. Nakamura, T. Motoki, GaN substrate technologies for optical devices, P. IEEE 101 (2013) 2221–2228.
[53] N. Gmeinwieser, U. Schwarz, Pattern formation and directional and spatial ordering of edge dislocations in bulk GaN: microphotoluminescence spectra and continuum elastic calculations, Phys. Rev. B75 (2007) 245213.
[54] A.H. Cottrell, Dislocations and Plastic Flow in Crystals, Clarendon, Oxford, 1963.
[55] D. Hull, D.J. Bacon (Eds.), Introduction to Dislocations, fifth ed., Elsevier, Amsterdam, 2011.
[56] J.J. Derby, A. Yeckel, Heat transfer analysis and design for bulk crystal growth: perspectives on the Bridgman method, in: T. Nishinaga, P. Rudolph, T. Kuech (Eds.), Handbook of Crystal Growth, Vol IIB, second ed., Elsevier, Amsterdam, 2015, pp. 793–844.
[57] V.L. Indenbom, Ein Beitrag zur Entstehung von Spannungen und Versetzungen beim Kristallwachstum, Cryst. Res. Technol. 14 (1979) 493–507 (see also: A.A. Chernov, Modern Crystallography III, Springer Series in Solid-State Sciences, Vol. 36, Springer, Heidelberg, 1984).
[58] H. Alexander, P. Haasen, Dislocations and plastic flow in the diamond structure, Solid State Phys. 22 (1968) 27–158.

[59] N. Miyazaki, Thermal stress and dislocations in bulk crystal growth, in: T. Nishinaga, P. Rudolph, T. Kuech (Eds.), Handbook of Crystal Growth, Vol IIB, second ed., Elsevier, Amsterdam, 2015, pp. 1049–1093.

[60] V. Prasad, S. Pendurti, Models for stress and dislocation generation in melt-based compound crystal growth, in: G. Dhanaraj, K. Byrappa, V. Prasad, M. Dudley (Eds.), Springer Handbook of Crystal Growth, Springer, Heidelberg, 2010, pp. 1335–1378.

[61] L.P. Kubin, Dislocations, Mesoscale Simulations and Plastic Flow, Oxford Series of Materials Modelling, Oxford Univ., 2013.

[62] J. Winkler, M. Neubert, Automation of crystal growth from melt, in: T. Nishinaga, P. Rudolph, T. Kuech (Eds.), Handbook of Crystal Growth, Vol IIB, second ed., Elsevier, Amsterdam, 2015, pp. 1143–1184.

[63] M. Naumann, P. Rudolph, M. Neubert, J. Donecker, Dislocation studies in VCz GaAs by laser scattering tomography, J. Cryst. Growth 231 (2001) 22–33.

[64] G. Grange, C. Jourdan, A.L. Coulet, J. Gastaldi, Observation of the melting-solidification processes of an Al crystal by synchrotron X-ray topography, J. Cryst. Growth 72 (1985) 748.

[65] B. Bako, I. Groma, G. Györgyi, G. Zimanyi, Dislocation patterning: the role of climb in meso-scale simulations, Comput. Mater. Sci. 38 (2006) 22–28.

[66] P. Rudolph, F.-M. Kiessling, Growth and characterization of GaAs crystals produced by the VCz method without boric oxide encapsulation, J. Cryst. Growth 292 (2006) 532–537.

[67] R.J. Amodeo, N.M. Ghoniem, Dislocation dynamics. I. A proposed methodology for deformation micromechanics, Phys. Rev. B 41 (1990) 6958–6967.

[68] S.V. Raj, G.M. Pharr, A compilation and analysis of data for the stress dependence of the subgrain size, Mater. Sci. Eng. 81 (1986) 217–237.

[69] C. Frank-Rotsch, U. Juda, F.-M. Kiessling, P. Rudolph, Dislocation patterning during crystal growth of semiconductor compounds (GaAs), Mater. Sci. Technol. 21 (2005) 1450–1454.

[70] G. Grange, C. Jourdan, J. Gastaldi, B. Billia, Stresses and defects in the formation of a cellular pattern in directional solidification. Real-time observation by synchrotron X-ray topography on a Al-0.73 wt% Cu alloy, J. Phys. III 4 (1994) 293–304.

[71] H. Klapper, Generation and propagation of defects during crystal growth, in: G. Dhanaraj, K. Byrappa, V. Prasad, M. Dudley (Eds.), Springer Handbook of Crystal Growth, Springer, Heidelberg, 2010, pp. 93–131.

[72] M. Shibata, T. Suzuki, S. Kuma, T. Inada, LEC growth of large GaAs single crystals, J. Cryst. Growth 128 (1993) 439–443.

[73] C.F. Johnston, M.J. Kappers, C.J. Humphreys, Microstructural evolution of nonpolar (11–20) GaN grown on (1–102) sapphire using a 3D-2D method, J. Appl. Phys. 105 (2009) 073102.

[74] C.-P. Chu, S. Arafin, T. Nie, K. Yao, X. Kou, L. He, et al., Nanoscale growth of GaAs on patterned Si(111) substrates by molecular beam epitaxy, Cryst. Growth Des. 14 (2014) 593–598.

[75] S. Luryi, E. Suhir, New approach to the high quality epitaxial growth of lattice-mismatched materials, Appl. Phys. Lett. 49 (1986) 140–142.

[76] Y. Kato, S. Kitamura, K. Hiramatsu, N. Sawaki, Selective growth of wurtzite GaN and $Al_xGa_{1-x}N$ on GaN/sapphire substrates by metalorganic vapor phase epitaxy, J. Cryst. Growth 144 (1994) 133.

[77] M. Alimoradi Jazi, T. Meisch, M. Klein, F. Scholz, Defect reduction in GaN regrown on hexagonal mask structure by facet assisted lateral overgrowth, J. Cryst. Growth 429 (2015) 13–18.

[78] W.D. Nix, B.M. Clemens, Crystallite coalescence: a mechanism for intrinsic tensile stresses in thin films, J. Mater. Res. 14 (1999) 3467–3473.

[79] C. Lan, C. Hu, K. Nakajima, Multicrystalline silicon crystal growth for photovoltaic, in: T. Nishinaga, P. Rudolph, T. Kuech (Eds.), Handbook of Crystal Growth, Vol IIA, second ed., Elsevier, Amsterdam, 2015, pp. 373–412.

[80] M. Shibata, Y. Sasaki, T. Inada, S. Kuma, Observation of edge-facets in <100> InP crystals grown by LEC method, J. Cryst. Growth 102 (1990) 557–561.

[81] V.V. Voronkov, Processes at the boundary of a crystallization front, Sov. Phys. Crystallogr. 19 (1975) 573–577.

[82] H. Gottschalk, G. Patzer, H. Alexander, Stacking fault energy and ionicity of cubic III–V compounds, Physica Status Solidi A Appl. Res. 45 (1978) 207–217.

[83] D.T.J. Hurle, A mechanism for twin formation during Czochralski and encapsulated vertical Bridgman growth of III-V compound semiconductors, J. Cryst. Growth 147 (1995) 239–250.

[84] X. Li, R. Yang, F. Yang, T. Sun, N. Sun, Influence of the cone angle and crystal shape on the formation of twins in InP crystals, Phys. Status Solidi C 9 (2012) 165–168.

[85] M. Neubert, A. Kwasniewski, R. Fornari, Analysis of twin formation in sphalerite-type compound semiconductors: a model study on bulk InP using statistical methods, J. Cryst. Growth 310 (2008) 5270–5277.

[86] P. Rudolph, A. Engel, I. Schentke, A. Grochocki, Distribution and genesis of inclusions in CdTe and (Cd,Zn)Te single crystals grown by the Bridgman method and by the travelling heater method, J. Cryst. Growth 147 (1995) 297–304.

[87] P. Rudolph, M. Neubert, M. Mühlberg, Defects in CdTe Bridgman monocrystals caused by nonstoichiometric growth conditions, J. Cryst. Growth 128 (1993) 582–587.

[88] C.H. Henager, K.J. Alvine, M.Y. Bliss, B.J. Riley, J.A. Stave, The influence of constitutional supercooling on the distribution of Te-particles in melt-grown CZT, J. Electron. Mater. 44 (2015) 4604–4621.

[89] T. Steinegger, M. Naumann, M. Jurisch, J. Donecker, Precipitate engineering in GaAs studied by laser scattering tomography, Mater. Sci. Eng. B Solid State Mater. Adv. Technol. 80 (2001) 215–219.

[90] A.A. Chernov, D.E. Temkin, Capture of inclusions in crystal growth, in: E. Kaldis, H.J. Scheel (Eds.), Current Topics of Materials Science: Crystal Growth and Materials, vol. 2, North-Holland, Amsterdam, 1977, pp. 3–77.

[91] O.P. Fedorov, Interaction between growing crystals and inclusions in the melt, J. Cryst. Growth 102 (1990) 857–861.

[92] H. Aufgebauer, J. Kundin, H. Emmerich, M. Azizi, C. Reimann, J. Friedrich, et al., Phase-field simulations of particle capture during the directional solidification of silicon, J. Cryst. Growth 446 (2016) 12–26.

[93] S. Hu, C.H. Henager, Phase-field simulations of Te-precipitate morphology and evolution kinetics in Te-rich CdTe crystals, J. Cryst. Growth 311 (2009) 3184–3194.

[94] R.D.S. Yadava, R.K. Bagai, W.N. Borle, Theory of Te precipitation and related effects in CdTe crystals, J. Electron. Mater. 21 (1992) 10011016.